

Chapter 1

Overview of tropical cyclones and historical perspective

Wenchang Yang¹, Emma Levin², Sofia Menemenlis², Nicoló Scapin³, Michael Igbinoba¹, Maya Chung², Gabriel Rios², Tsung-Lin Hsieh², Luc Deike⁴, Ivan Mitevski¹ and Gabriel A. Vecchi⁵

¹Department of Geosciences, Princeton University, Princeton, NJ, United States, ²Program in Atmospheric and Oceanic Sciences, Princeton University, Princeton, NJ, United States, ³High Meadows Environmental Institute, Princeton University, Princeton, NJ, United States, ⁴Department of Mechanical and Aerospace Engineering and the High Meadows Environmental Institute, Princeton University, Princeton, NJ, United States,

⁵Department of Geosciences and the High Meadows Environmental Institute, Princeton University, Princeton, NJ, United States

1.1 Introduction

Tropical cyclones (TCs), the fast rotating and low pressure–centered storm systems emerging from the tropics, are the most hazardous type of weather phenomena and impact areas proximal to the Pacific, North Atlantic, and Indian Oceans. TCs are seasonal but irregular phenomena, forming in otherwise hospitable tropical climates and capable of violent destruction on people and ecosystems. The impacts of each TC are different, but are felt through some combination of strong winds, heavy rain, and storm surge.

The destructive character of TCs has been understood for centuries through local knowledge systems. In Mesoamerica and the Caribbean, for example, indigenous people regarded gods capable of unleashing strong rotating winds and rain: the God “Hurakán,” or “Heart of Sky,” is a central figure in the creation story recorded in the Mayan *Popol Vuh* ([Popol Vuh: The Sacred Book of Maya, 2007](#)), and the Taíno deity Guabancex is a mistress of winds depicted with curved arms swirling around her face like rain bands in a TC ([Schwartz, 2015](#), pp. 6–7).

Today, new ways of observing and understanding TCs rely on technologies developed largely since World War II. Reconnaissance aircraft, meteorological radar, and Earth-observing satellites are used to measure the location, movement, winds, pressure, temperature, and humidity of these storms. We can now use numerical weather prediction models to predict TCs and issue warnings days in advance, and to study small-scale phenomena within storms (e.g., [Harris et al., 2020](#); [Menemenlis et al., 2024](#); [Zhou et al., 2019](#)). Global climate models with sufficiently high resolution can represent the TC climatology over hundreds of years, and are used to research the relationship between these storms and climate.

TCs are a general phenomenon of the global tropics, but are also referred to by distinct regional names in English. An Atlantic or Eastern Pacific TC is called a hurricane, from the Spanish *huracán*. *Huracán* may have been borrowed from indigenous languages, though some sources have attributed it to Spanish or Latin origins ([Schwartz, 2015](#), p. 7). A western Pacific TC is called a typhoon, a Cantonese loanword that may have been previously transmitted by Arabic and derived from Greek ([Cannon & Kaye, 1994](#)), although the etymology is debated.

In many countries, national meteorological agencies assume a level of responsibility for monitoring, forecasting, and issuing warnings of threats from TCs. Regional organizations, notably the World Meteorological Organization’s TC regional bodies, facilitate the sharing of information, knowledge, and technology. Each unique TC is given a name, helping to facilitate public awareness and communication. These names are coordinated regionally and globally, with a different naming procedure in each region to ensure that names are unique, culturally appropriate, and easy to pronounce.

Although each storm has its own character, TCs share certain common characteristics. An area of clouds, rain, and strong winds spanning hundreds of kilometers in diameter swirls around a relatively calm “eye” spanning tens of kilometers across. TCs are cyclonic, rotating in the same direction as the planet—clockwise in the Southern Hemisphere and counterclockwise in the Northern Hemisphere. They last for days to weeks, and sometimes move thousands of kilometers across space before they dissipate or transform into extratropical storms.

This chapter will provide an overview of the fundamental characteristics of TCs, setting the stage for more in-depth discussions of their impacts in the rest of the book.

1.2 Tropical cyclone's structure, life cycle, kinematics, and energetics

In a typical TC (Fig. 1.1), wind vectors converge toward the center after passing through a very moist (purple) eyewall; this occurs due to the presence of relatively low pressure there. This center is most clearly highlighted not just by this convergence, but also by low relative humidity (light blue-brown) values compared to the surroundings that show the deep, dry warm core of the cyclone. Accordingly, thermal wind balance dictates that inflowing winds in the lower half of the troposphere are to be much stronger than the outflowing air near the top (Anthes, 1974).

Using outgoing infrared radiation converted to a brightness temperature (Fig. 1.2), we can clearly see the spirally organized clouds of a mature TC on the horizontal plane. Colder regions depict high-level cirrus canopy of stronger thunderstorms, while warmer regions show a much shallower to nonexistent cloud deck in all layers of the atmosphere.

Wind speed increases away from the center of a TC and peaks around the eyewall, the most turbulent region of a hurricane (Fig. 1.3). It is possible to see many perturbations in the wind field structure both inside and outside of the maximum wind ring from smaller-scale convective features (note the kinks in eyewall winds, which are a result of such features).

The development of a TC is one of the most fascinating processes in nature. In general, the process begins as the organization of disturbances in the tropics, followed by the development of an organized, cyclonically rotating vortex that possesses notable depth in the troposphere. Unlike the midlatitude weather, which is often driven by synoptic-scale systems, tropical disturbances are less organized. Occasionally, these disturbances may acquire sufficient vorticity, for instance through the instability of tropical waves, forming a vortex that can be identified on a weather map.

The intensification of an incipient vortex into a tropical storm, and when conditions are right, a hurricane, is characterized by the increase in surface wind speed, decrease in central surface pressure, and increase in core temperature relative to the environment. Several physical processes determine the strengthening or weakening of the vortex. With the aid of observations and computer simulations, much progress has been made in understanding the dynamics and thermodynamics of TC development.

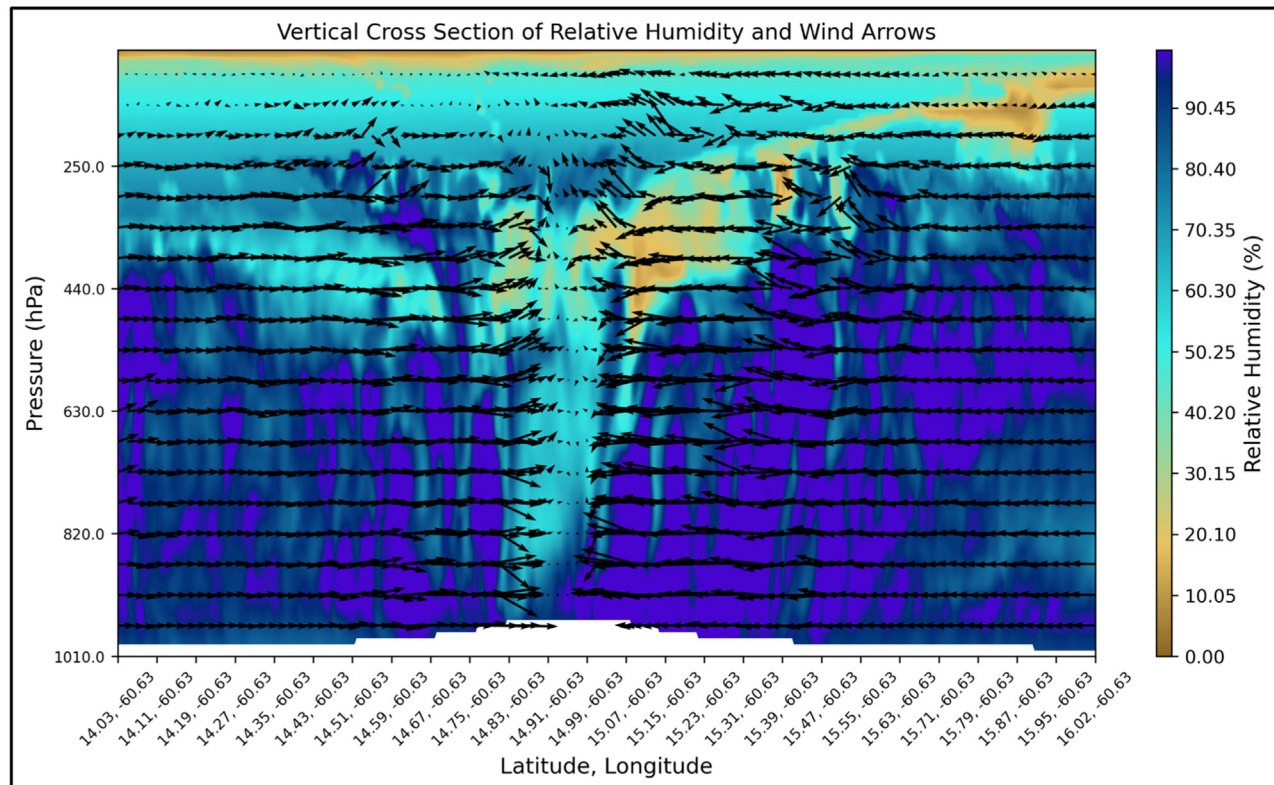


FIGURE 1.1 Vertical cross section of relative humidity and wind arrows from a high-resolution simulation of a mature tropical cyclone.

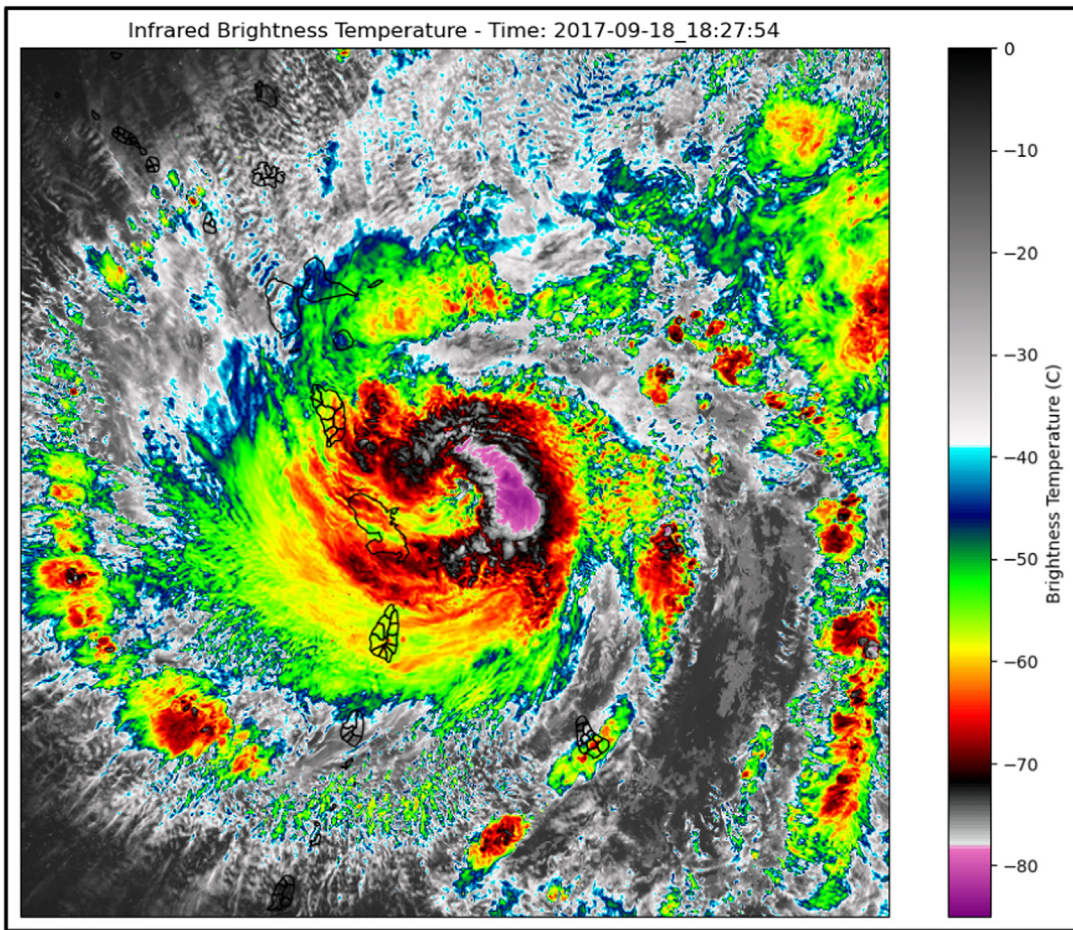


FIGURE 1.2 Infrared brightness temperature from a high-resolution simulation of a mature tropical cyclone.

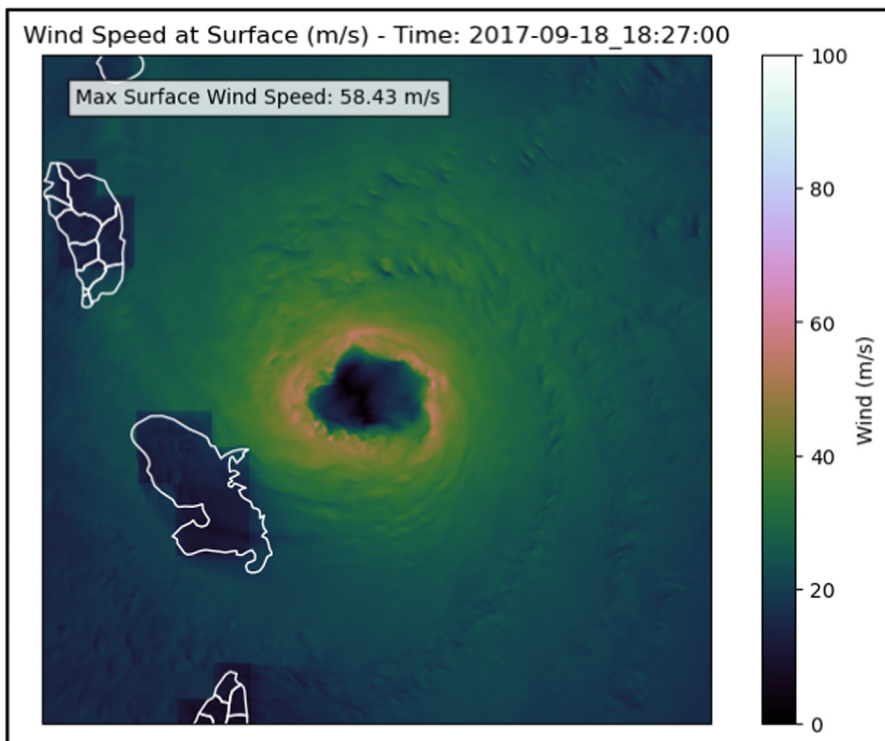


FIGURE 1.3 Horizontal wind speed at surface from a high-resolution simulation of a mature tropical cyclone.

4 Tropical Cyclones and Associated Impacts

It is useful to characterize different stages of TC development based on the relative importance of processes in physical equations. In the energetics equation, disorganized tropical disturbances are more sensitive to the radiative effects of clouds, while organized vortices are more sensitive to surface fluxes induced by the stronger surface winds (Wing et al., 2019; Zhang et al., 2021). In the vorticity equation, the effect of the Earth's curvature is more important than the stretching effect to the disturbances, but the stretching effect becomes more important as the vortex is formed and expanded (Hsieh et al., 2020; Lu & Chavas, 2022). This newly formed vortex is typically weaker than a TC, hence referred to as a TC "seed."

The spinning seed vortex continues to be fueled by surface fluxes and intensifies into a TC (Rotunno & Emanuel, 1987). It does not intensify indefinitely though. The directional and/or magnitudinal change of horizontal winds with height, or vertical wind shear, can ventilate lower energy and entropy air from the environment into the core of the vortex and limit the growth of the cyclone (Rappin et al., 2010; Tang & Emanuel, 2010). Another limiting effect comes from surface friction, which becomes more influential as the surface wind speed increases. Therefore a TC tends to intensify over warm oceans, which provide sufficient energy and entropy, while it dissipates when cold and dry air is ventilated into the storm. In the process, the cyclone transfers kinetic energy into the ocean and land surfaces as it moves, causing serious damage to lives and properties as it makes landfall.

The potential for damage to lives and properties increases when TCs move poleward. These storms generally move poleward (northward in the Northern Hemisphere, southward in the Southern Hemisphere) due to environmental steering factors and the beta effect (Chan, 2005a). Examples of environmental steering factors include the trade winds, upper-tropospheric jets, and synoptic-scale flow driven by large-scale pressure gradients (such as the southeasterly winds driven by the Azores High in the North Atlantic). The beta effect occurs when a synoptic-scale system, such as TCs, experiences a difference in planetary vorticity over their meridional extent. This vorticity gradient contributes to storm steering, with storms in the Northern (Southern) Hemisphere experiencing northwestward (southeastward) drift (Wang et al., 1997). However, it should be noted that relative to other steering factors, beta drift tends to have weaker effects; as a consequence of the meridional planetary vorticity gradient, beta drift magnitude is also dependent on the size and intensity of the storm. The poleward motion of TCs leads to storm motion out of the tropics and into higher latitudes, where they lose tropical characteristics (i.e., the warm core cools, surface fluxes weaken due to cooling sea surface temperatures, or SSTs) and often merge with powerful extratropical cyclones or combine with extratropical troughs to form these strong cyclones (Jones et al., 2003; Klein et al., 2000). The transition of a TC into an extratropical system also results in the broadening of the low-pressure system, leading to a significantly larger wind field.

Extratropically transitioning TCs (abbreviated as ETTCs) present significant impacts to life and property given the increases in storm size and the intensification of storms in the midlatitudes. Therefore ETTCs serve to extend the meridional extent of TC impacts to regions not directly affected by these systems. These impacts often appear in the form of distributed and intense precipitation and large areas of gale-force winds. The northeastern United States is an example of an area affected by these impacts; Hurricane Floyd (1999) and Irene (2011) contributed to extreme rainfall and prolonged gusts over highly urbanized areas that led to widespread property damage (Colle, 2003; Liu & Smith, 2016). Additionally, the increased low-pressure area and broader wind fields in ETTCs amplify storm surge magnitudes and extent, resulting in increased coastal flooding risk (Nederhoff et al., 2024; Orton et al., 2016); the impacts of Hurricanes Irene (2011) and Sandy (2012) on the New York City metropolitan area are prominent examples of this risk. Due to the impacts of anthropogenic warming, the frequency of ETTCs is projected to increase over the 21st century due to an expansion of tropical cyclogenesis' latitudes and the increased transport of tropical characteristics into higher latitudes (Liu et al., 2017; Liu et al., 2018). This implies the potential for exacerbated risks to regions not typically exposed to TC conditions.

1.3 Measures of tropical cyclone intensity and activity

Meteorologists, climate scientists, and engineers have developed metrics to classify several important TC characteristics. Doing so enables them to compare TCs across different basins and time periods, to study the time evolution of TCs, and to clearly communicate potential TC impacts to the public. Below are five widely used indices that describe storm strength, activity, and destructiveness.

1.3.1 Measures of intensity and destructiveness

Civil engineer Herbert Saffir and meteorologist Robert Simpson developed the **Saffir–Simpson scale** in 1971 to classify hurricanes into five different categories solely based on their maximum surface wind speed. The categories are labeled one through five, with increasing wind speeds and potential wind-related damage associated with the higher category numbers (National Hurricane Center, 2021). A hurricane attaining Category 1 status, for instance, experiences

TABLE 1.1 The Saffir–Simpson scale, each level's associated maximum wind speeds, and the potential damage imposed due to the strength of the winds.

Category	Maximum winds	Wind-related hurricane damage
1	74–95 mph, 64–82 kt, 119–153 km h ⁻¹	Very dangerous winds will produce some damage: Well-constructed frame homes could have damage to roof, shingles, vinyl siding, and gutters. Large branches of trees will snap and shallowly rooted trees may be toppled. Extensive damage to power lines and poles will likely result in power outages that could last a few to several days.
2	96–110 mph, 83–95 kt, 154–177 km h ⁻¹	Extremely dangerous winds will cause extensive damage: Well-constructed frame homes could sustain major roof and siding damage. Many shallowly rooted trees will be snapped or uprooted and block numerous roads. Near-total power loss is expected with outages that could last from several days to weeks.
3	111–129 mph, 96–112 kt, 178–208 km h ⁻¹	Devastating damage will occur: Well-built framed homes may incur major damage or removal of roof decking and gable ends. Many trees will be snapped or uprooted, blocking numerous roads. Electricity and water may be unavailable for several days to weeks after the storm passes.
4	130–156 mph, 113–136 kt, 209–251 km h ⁻¹	Catastrophic damage will occur: Well-built framed homes can sustain severe damage with loss of most of the roof structure and/or some exterior walls. Most trees will be snapped or uprooted and power poles downed. Fallen trees and power poles will isolate residential areas. Power outages will last weeks to possibly months. Most of the area will be uninhabitable for weeks or months.
5	157 mph, 137 kt, 252 km h ⁻¹	Catastrophic damage will occur: A high percentage of framed homes will be destroyed, with total roof failure and wall collapse. Fallen trees and power poles will isolate residential areas. Power outages will last for weeks to possibly months. Most of the area will be uninhabitable for weeks or months.

Source: Directly reproduced from the National Oceanographic and Atmospheric Administration National Hurricane Center. <https://www.nhc.noaa.gov/aboutshws.php>.

maximum wind speeds of 74–95 mph and is associated with potential damage to a home's roof, shingles, and gutters. A hurricane attaining Category 4 status, on the other hand, experiences maximum wind speeds of 130–156 mph and is associated with a significant loss of a home's roof structure and high wind speeds (Table 1.1).

A hurricane's classification using the Saffir–Simpson scale is instantaneous in time and space as a hurricane can change classification along its trajectory. For example, Hurricane Katrina (2005) inflicted overwhelming damage and life loss along the coast of the Gulf of Mexico. The storm initially made landfall in Florida as a Category 1 hurricane (sustaining maximum wind speeds of 80 mph). Several days later, after moving into the very warm Gulf of Mexico, the storm intensified to a Category 5 hurricane (sustaining maximum winds of 175 mph).

Although the Saffir–Simpson scale provides a widely used mechanism to assess the wind speed intensity and wind-related damage across all hurricanes, this metric has several flaws. First, it does not address hurricane-related hazards unrelated to wind, including heavy rainfall-induced flooding and storm surge. For instance, when Hurricane Sandy (2012) made landfall in New York City, it sustained Category 1 winds, the lowest Saffir–Simpson classification. However, the associated flooding in New York City surpassed 8.5 ft., a catastrophic flood height with a 400-year return period (Lin et al., 2016). The Saffir–Simpson scale alone cannot foresee all of a hurricane's potential damages.

Additionally, the Saffir–Simpson scale is a rigid quantification using hurricane wind speeds, which does not factor in the time evolution of hurricane wind speeds. As discussed in Section 1.7, hurricane wind speeds are projected to intensity as the global climate warms and might manifest in wind speeds exceeding the Category 5 threshold. One study proposes defining a sixth category for hurricanes with a high level of wind hazard (Wehner & Kossin, 2024).

Lastly, the locality of a Saffir–Simpson scale limits the ability to assess a hurricane's strength along its full trajectory. One metric created to synthesize a storm's total wind strength and duration is the **accumulated cyclone energy (ACE)** (Bell et al., 2000). ACE is calculated for a TC as follows:

$$\text{ACE} = 10^{-4} \sum_{\text{6 hourly}} v_{\max}^2, \text{ for } v_{\max} \geq 34 \text{ knots; } 63 \text{ km/h; } 39 \text{ mph,} \quad (1.1)$$

where the squared maximum winds of a storm every 6 hours are added together, given that the maximum winds are above a certain threshold (Gray, 1988). Atmospheric scientist William Gray developed a precursor to ACE in 1988, finding the total destructiveness of a storm is associated with the square of the maximum wind speed. To obtain an indicator of a basin's total seasonal TC wind destructiveness, one could sum the total ACE for all the seasonal TCs in the basin.

Similar to ACE, the **power dissipation index (PDI)**, developed by atmospheric scientist Kerry Emanuel in 2005, measures the wind-related hazard of a TC over its lifetime and has units of energy (Emanuel, 2005; Emanuel, 2007; Sun et al., 2017). PDI is calculated by integrating cubic wind speed over the TC's surface area throughout its duration,

$$\text{PDI} = 2\pi \int_0^T \int_0^R C_D \rho |V|^3 r dr dt, \quad (1.2)$$

where C_D is the drag coefficient, ρ is the density of air, $|V|$ is the magnitude of wind 10 m above the ground, and the integral is over radius to the outer boundary of the storm R and over time T , the storm's lifetime. There are two key differences between ACE and PDI. First, PDI integrates wind speed over the entire area of the storm, while ACE only comprises the maximum winds of the storm. Second, PDI places a higher weight on wind speed than ACE does. Wind speed magnitude is raised to the third power to calculate PDI, while wind speed is squared to calculate ACE. Emanuel argues that PDI is an accurate representation of storm destructiveness, given that monetary losses are proportional to the cube of the wind speed (Schwerdt et al., 1979). Although ACE and PDI provide a measure of storm strength along its full course, like the Saffir–Simpson scale, these metrics are primarily wind-based. They too do not account for storm surge or rainfall.

The TC intensity measures described thus far have been diagnostic. They provide information to scientists and the public about a storm's strength based on its observed conditions. The final measure of storm intensity, **Potential Intensity (PI)**, is a theoretical, prognostic measure. Based on the background environmental conditions in a TC basin and in the overlying atmosphere, PI posits a storm's theoretical maximum wind speed (Fig. 1.4), if the storm were to occur in such conditions (Emanuel, 1986; Emanuel, 1995; Holland, 1997). With an original goal of understanding the role of atmosphere–ocean interactions in hurricane strength, Emanuel created this measure in 1986. PI allows scientists to understand which basins can sustain TCs with a specified wind speed and to examine how these regions might change in the future. This metric is a function of atmospheric and oceanic temperature, as well as atmosphere–ocean heat exchanges (Bister & Emanuel, 1998).

1.3.2 Measures of damage

The Saffir–Simpson Scale, ACE, and PDI all measure TC wind-related damage. A key flaw of these indices is that they only measure wind-related TC hazards, not heavy rainfall or storm surge. To address this flaw, Klotzbach et al., (2020) argue that the instantaneous **minimum sea-level air pressure (MSLP)** at the center of a TC is a better covariate with total monetary storm-related losses than wind speeds. Like the Saffir–Simpson scale, Klotzbach et al. propose

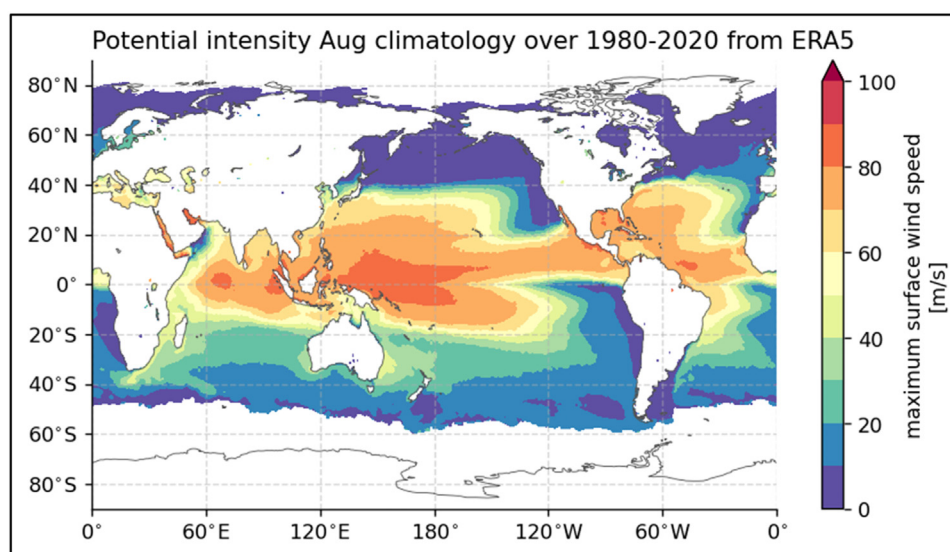


FIGURE 1.4 August climatology of potential intensity (PI) calculated from the ERA5 reanalysis data over the period of 1980–2020. PI is represented by maximum surface wind speed in units of m s^{-1} . PI exceeds 80 m s^{-1} in the Western Pacific Ocean and the Gulf of Mexico, which corresponds to potential maximum TC winds above 178 mph. Such wind speeds are classified as Category 5 hurricane wind speeds on the Saffir–Simpson scale. Map lines delineate study areas and do not necessarily depict accepted national boundaries.

using MSLP at each point along its trajectory as an indicator for total damages. Studies show that MSLP is highly correlated with maximum storm wind speeds, storm size, storm surge, and rainfall (Irish et al., 2008; Lonfat et al., 2007), which means this metric is more encompassing than the wind speed–based measures. MSLP is an easier feature to measure than wind speed, since pressure can readily be determined using a barometer, while standard anemometers might have difficulty accurately measuring TC-strength winds. Also, climate models tend to predict MSLP more accurately than winds. Calculating and projecting these indices can inform the public about potential TC-related losses and help vulnerable communities adequately prepare for TCs.

1.3.3 Measure of activity

Just as PI is a theoretical measure of potential TC maximum winds based on the environmental state, the **Genesis Potential Index (GPI)** calculates potential TC genesis as a function of large-scale background conditions. Several studies (Emanuel & Nolan, 2004; Gray, 1979; Tippett et al., 2011; Wang & Murakami, 2020) propose different formulas for the GPI based on distinct environmental variables. In all cases, a higher GPI corresponds to a higher TC genesis likelihood, thus higher storm activity. For example, one such GPI developed by (Emanuel & Nolan, 2004) is defined as

$$\text{GPI} = |10^5 \eta|^{3/2} (H/50)^3 (\text{PI}/70)^3 (1 + 0.1V)^{-2}, \quad (1.3)$$

where η is the absolute vorticity, a measure of rotational motion of the winds, H is a measure of humidity or moisture content in the atmosphere, PI is a measure of potential intensity as described above, and V is the difference in winds between the lower and upper atmosphere.

GPIs allow scientists to ask important questions about the influence of climate on TC activity. It remains difficult to simulate TCs in global numerical climate models, since these models are biased and often do not have a high enough resolution to simulate the complex processes required for cyclogenesis described in Section 1.1. Thus climate scientists often use the GPI as a proxy for TC activity to study its temporal and spatial evolution when TCs cannot be directly modeled numerically.

In addition, GPIs provide a conceptual framework that helps scientists understand how TCs are influenced by environmental variables. The development of TCs is a complex process that depends on the interaction between their internal structure and the external environment. Progress has been made in determining the relative importance of various environmental variables at different time scales and stages of TC development. For example, the Coriolis parameter is generally more important in the early stages when the TC has not yet developed sufficient vorticity (Emanuel, 2022). It is useful to group variables commonly used in GPIs, such as those listed above, in the following order by their influence on TC development stages (Hsieh et al., 2022):

$$\text{GPI}_H = (-\omega) \frac{1}{\sqrt{1 + Z^{-1.4}}} \frac{1}{\sqrt{1 + (0.014/\Lambda)^{-1.1}}}, \quad (1.4)$$

where ω is the mid-troposphere large-scale vertical velocity (minus represents large-scale ascent), $Z = \eta/\sqrt{\beta U}$ is a non-dimensional rotation parameter, $\Lambda = V\chi/\text{PI}$ is the nondimensional ventilation index, and χ is the nondimensional saturation deficit. The first two factors primarily determine the early stage development, influenced by the large-scale overturning circulation, radiation, and background vorticity (Hsieh et al., 2023; Rappin et al., 2010; Wing et al., 2016; Zhang et al., 2021). The last factor characterizes the competition between the intensifying effect of surface fluxes and the weakening effect of ventilation discussed in Section 1.2, which is more important in the later stage of TC development. In general, the change in large-scale ascent plays a bigger role in explaining how TC activity changes with the global climate (Chand et al., 2022; Hsieh et al., 2022; Murakami & Wang, 2022). For seasonal TC variability, it is the change in vertical wind shear, a term in the ventilation index, that is more important (Yang et al., 2021).

The Saffir–Simpson Scale, ACE, PDI, PI, and GPI are metrics that are used to describe TC features. These measures are important both for scientific study of TC behavior and for the communication of TC hazards to the public.

1.4 Tropical cyclone climatology

Globally, around 80 TCs occur each year, with a standard deviation of approximately 7, according to best track records (Fig. 1.5). The Northern Hemisphere experiences around 70% of global TCs. The most active basin for TCs is the Western North Pacific, where nearly a third of global TCs originate (~ 26 storms a year). The Eastern North Pacific sees 16.9 storms a year, and the North Atlantic experiences 13.4. The South Indian, Australian, and South Pacific TC

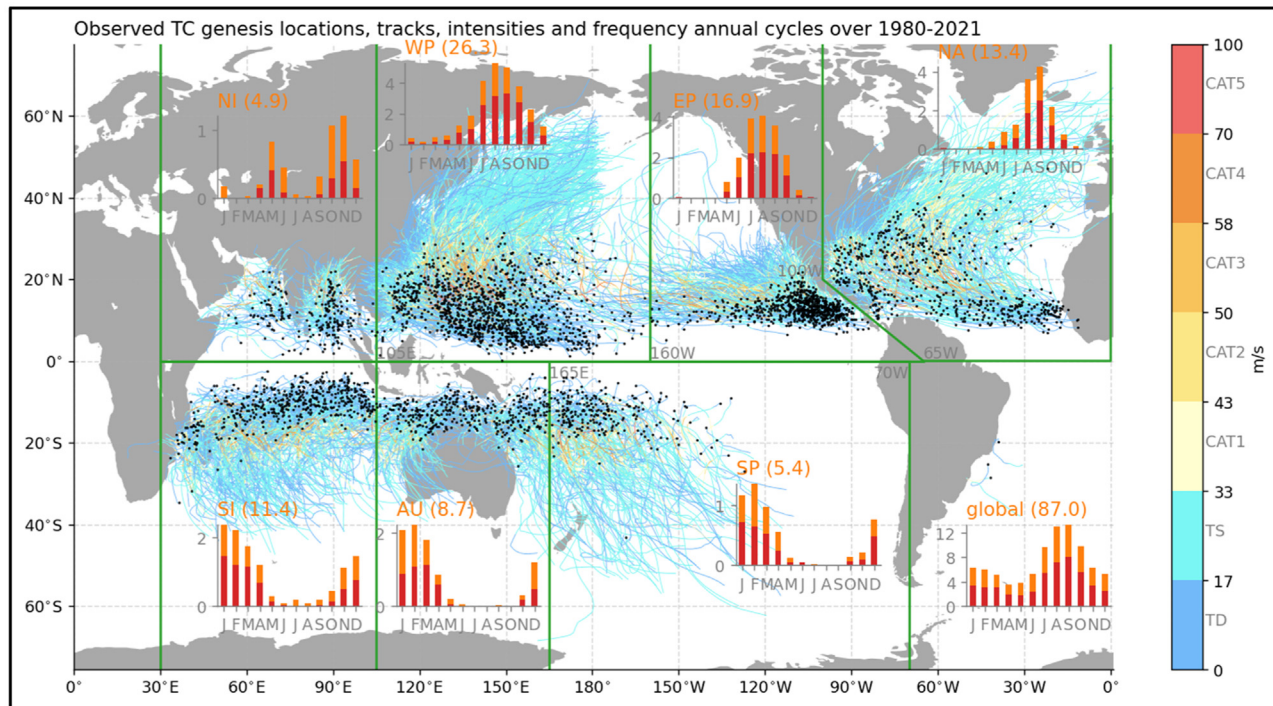


FIGURE 1.5 Observed tropical cyclone (TC) genesis locations (black dots), tracks (color lines), intensities (in units of m s^{-1} using a color map from the color bar on the right), and frequency annual cycles (bars) from version 4 of IBTrACS over the years 1980–2021. TC frequency annual cycles (bars) are shown for the global (bottom right bar plot) as well as the seven TC basins: North Atlantic (NA), East Northern Pacific (EP), West Northern Pacific (WP), North Indian (NI), South Indian (SI), Australian (AU), and South Pacific (SP). In each of the annual cycle bar plots, TCs at the intensity level of tropical storms (TS) and hurricanes (HU) are in orange and red, respectively. The annual average number of TCs (both TS and HU) in each basin or global scale are also shown after the basin name in each bar plot. Map lines delineate study areas and do not necessarily depict accepted national boundaries.

basins see 11.4, 8.7, and 5.4 TCs per year, respectively, while the North Indian Ocean only 4.9 TCs per year. The South Atlantic is not considered a TC basin because TCs there are exceptionally rare (Ramsay, 2017).

TC numbers usually peak in the warm season in each basin when the SST is high and the air is moist (Fig. 1.5), with the exception of the North Indian Basin, where TCs are largely suppressed during the summer monsoon season mainly due to strong vertical wind shear. As a result, North Indian TCs show a bimodal annual cycle, with the two peaks before and after the summer monsoon season (Fig. 1.5). Due to the dominance of the Northern Hemispheric TCs, the global TC annual cycle also peaks during the boreal summer and early fall. The drivers of TC annual cycles include both thermal and dynamical processes, with the role of variation of pre-TC seeds (i.e., vortices that have the potential to develop into TCs) highlighted in recent studies (Yang et al., 2021).

1.5 Tropical cyclone intraseasonal variability

TCs are modulated by a variety of climate modes on the intraseasonal time scale, which is often defined as 30–90 days in the literature but extended here to also cover the window of two weeks to a month. The most pronounced intraseasonal climate mode, the Madden and Julian Oscillation (MJO), was first reported in (Xie et al., 1963) and later described comprehensively in (Madden & Julian, 1972), from which the current name of the mode was coined. MJO is characterized by eastward propagation of large-scale enhanced and suppressed convection and rainfall in the tropics, which usually starts from the western Indian Ocean and dies out in the central Pacific Ocean, with the whole cycle about 30–90 days.

Similar to MJO, the Boreal Summer Intraseasonal Oscillation (BSISO; Kikuchi, 2021) also has a time scale of 30–90 days. However, BSISO is dominant in boreal summer (while MJO is dominant in boreal winter) and also has remarkable propagation in the northward direction besides the eastward propagation that is characteristic for MJO. The MJO and BSISO impact the TC genesis and development through the perturbation of the associated thermal and wind fields (Fowler & Pritchard, 2020; Klotzbach & Oliver, 2015).

Another intraseasonal climate mode, called the quasi-biweekly oscillation (QBWO; Chatterjee & Goswami, 2004; Murakami, 1976), has a shorter period of 10–20 days. The QBWO is one of the main controls on the active and break cycles of the Asian monsoon and also has an important influence on TCs, with convectively active phase more favorable for TC genesis than its inactive phase (You et al., 2019). While the MJO, BSISO, and QBWO are dominant over the tropics, Rossby wave breaking (RWB) is the climate variability from the extratropics. Some recent studies have found that RWB can reduce the North Atlantic TC activity through the intrusion of dry and cold air and increased vertical wind shear over the tropical and subtropical Atlantic basin (Zhang et al., 2017).

Modulation of TCs by intraseasonal climate modes provides sources of predictability of TCs on time scales beyond the two weeks from traditional weather forecast. Much progress of TC predictability has been made through projects of the Subseasonal to Seasonal (S2S; Vitart & Robertson, 2018) and Subseasonal Experiment (SubX; Pegion et al., 2019). Operational forecasts of TCs on the intraseasonal time scale have been established in many centers across the globe, including the National Oceanic and Atmospheric Administration (NOAA) Climate Prediction Center (CPC), European Centre for Medium-Range Weather Forecasts (ECMWF), Australian Bureau of Meteorology (BoM), Colorado State University (CSU), Joint Typhoon Warning Center (JTWC), and U.S. Naval Research laboratory (Camargo et al., 2019; Schreck et al., 2023).

1.6 Tropical cyclone interannual variability

TCs exhibit substantial variability from year to year, both globally and within ocean basins. Fig. 1.6 illustrates the interannual variability of TC frequency in each ocean basin and globally. Although the interannual variability of TC frequency is a similar amount at the global level and within individual ocean basins (Frank & Young, 2007), interannual changes in TC characteristics including frequency, genesis location, tracks, intensity, and rapid intensification differ across ocean basins. This is because different basins' climates respond differently to modes of interannual climate variability, and environmental controls on TCs differ among ocean basins.

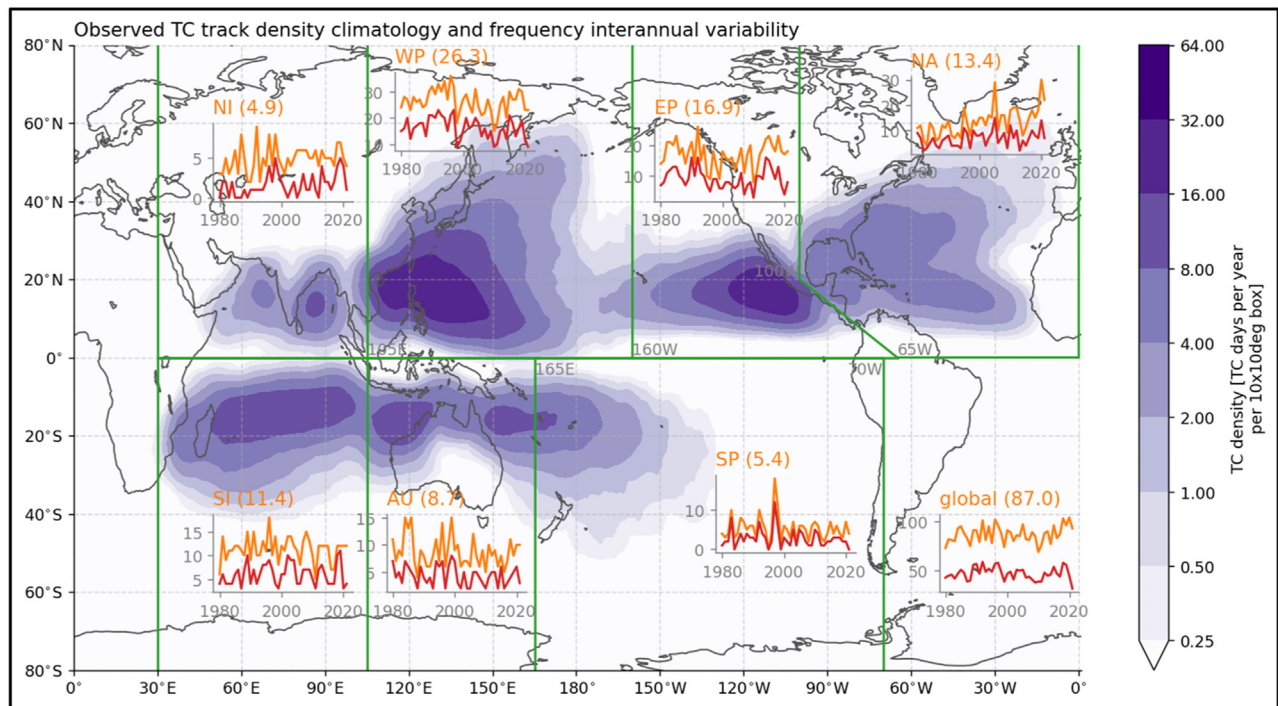


FIGURE 1.6 Observed tropical cyclone (TC) track density climatology (shaded), and annual TC number time series (or frequency, lines in each subplot) from version 4 of IBTrACS over the years 1980–2021. TC frequency annual time series (bars) are shown for the global (bottom right subplot) as well as the seven TC basins: North Atlantic (NA), East Northern Pacific (EP), West Northern Pacific (WP), North Indian (NI), South Indian (SI), Australian (AU), and South Pacific (SP). In each of the subpanels, TCs at the intensity level of tropical storms (TS) and hurricanes (HU) are in orange and red, respectively. The annual average number of TCs (both TS and HU) in each basin or global scale are also shown after the basin name in each bar plot. Map lines delineate study areas and do not necessarily depict accepted national boundaries.

On the interannual time scale, TCs can be impacted by abrupt radiative forcings (e.g., volcanic eruptions, Yang et al., 2019), but the dominant driver of TC interannual variability is the El Niño–Southern Oscillation (ENSO). ENSO is a naturally occurring climate mode with an approximately 2–7-year period, with warm (El Niño) and cold (La Niña) events lasting for about a year. ENSO modulates oceanic and atmospheric variables relevant to TC formation and strength across the globe. El Niño (La Niña) events are associated with warmer (colder) than usual SSTs and anomalously higher (lower) heat content in the upper ocean of the tropical Pacific, which can impact TC formation and intensity (Camargo & Sobel, 2005; Emanuel & Nolan, 2004; Murakami et al., 2015; Vecchi et al., 2014). ENSO can also alter the locations of tropical convection, the Intertropical Convergence Zone, subtropical highs, and large-scale atmospheric circulations such as the Walker and Hadley circulations (Lin et al., 2020). These atmospheric changes can impact vertical wind shear, atmospheric stability, humidity, and background vorticity, which can strengthen or suppress TCs and change their locations.

ENSO influences TCs across the globe through atmospheric teleconnections, and its impacts vary among ocean basins. In the North Atlantic basin, TCs tend to decrease in frequency (e.g., Gray, 1984) and intensity during El Niño due to higher vertical wind shear and atmospheric stability, and increase in frequency during La Niña (Ramsay, 2017; Tang & Neelin, 2004). In the western North Pacific and South Pacific basins, in contrast, TC frequency increases during El Niño and decreases during La Niña, and the locations of TC genesis also shift during ENSO events (e.g., Chan, 1985; Chan, 2005b; Dowdy et al., 2012).

Although El Niño and La Niña are often thought of as opposites, their impacts on climate and TCs are not perfect opposites. Fig. 1.7 illustrates the impacts of El Niño and La Niña on TC days in each basin. Note that El Niño and La Niña are associated with opposing effects in some but not all locations, and often the magnitude and locations of the effects differ.

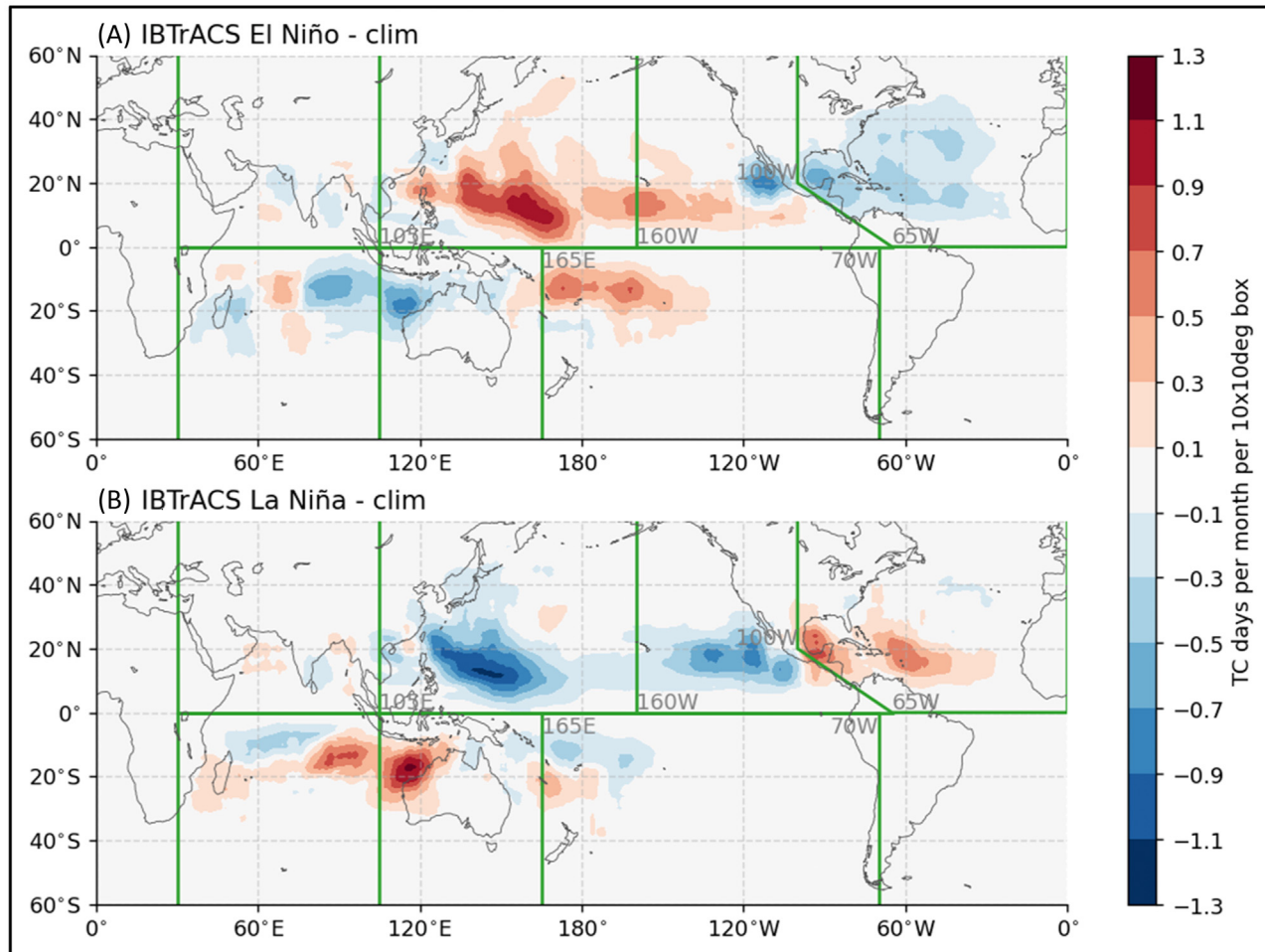


FIGURE 1.7 Tropical cyclone track density anomaly maps during May–November in the Northern Hemisphere and October–May in the Southern Hemisphere. (A) El Niño years minus 1980–2021 climatology. (B) La Niña years minus 1980–2021 climatology. Map lines delineate study areas and do not necessarily depict accepted national boundaries. Data source: IBTrACSv04r00.

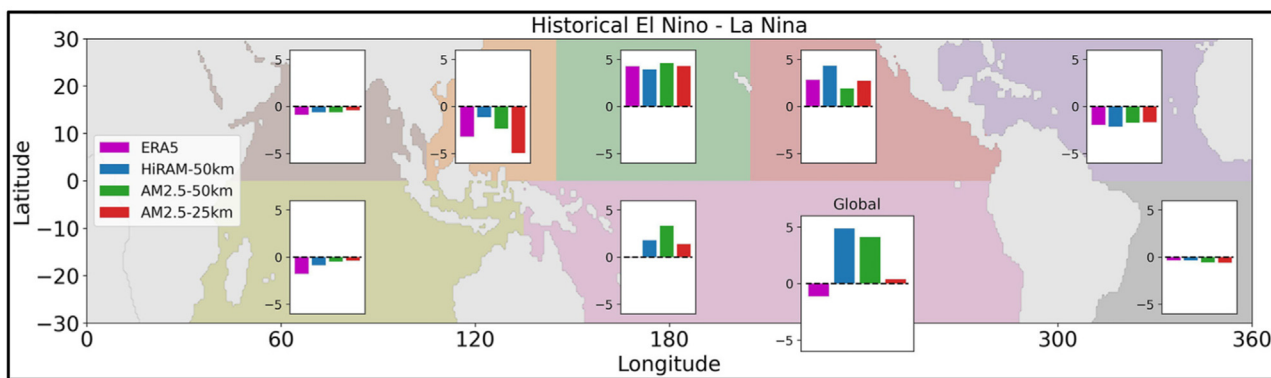


FIGURE 1.8 Basin contributions to the global percentage change in seed propensity index, a measure of the likelihood for seeds to occur, during El Niño years compared to La Niña years. Averaged over the nine strongest El Niño years and the seven strongest La Niña years between 1980 and 2015. Fig. 1.2c from Hsieh, T. L., Yang, W., Vecchi, G. A., & Zhao, M. (2022). Model spread in the tropical cyclone frequency and seed propensity index across global warming and ENSO-like perturbations. *Geophysical Research Letters*, 49 (7), [http://agupubs.onlinelibrary.wiley.com/hub/journal/10.1002/\(ISSN\)1944-8007.https://doi.org/10.1029/2021GL097157](http://agupubs.onlinelibrary.wiley.com/hub/journal/10.1002/(ISSN)1944-8007.https://doi.org/10.1029/2021GL097157).

The interannual variability of TC frequency is also in part due to the variability in the number of seeds that may eventually develop into TCs (Hsieh et al., 2022). Fig. 1.8 shows how the potential for seeds to form changes during El Niño compared to La Niña in each ocean basin and globally. Different ocean basins exhibit different signs and magnitudes of changes, but the changes tend to align between climate models and observations within basins.

Meridional climate modes can also impact the interannual variability of TCs and interact with ENSO. The Atlantic Meridional Mode (AMM) and the Pacific Meridional Mode (PMM) are variations of the meridional gradient in SSTs and surface winds in the tropical Atlantic and Pacific. The AMM and PMM vary on seasonal to decadal timescales, and the decadal part is thought to be the influence of decadal climate modes (e.g., Atlantic Multidecadal Oscillation; Vimont & Kossin, 2007). Positive correlation is found between the AMM and several TC intensity metrics in the North Atlantic (Vimont & Kossin, 2007), while negative correlation is found between AMM and TC counts in the Western North Pacific (Zhang et al., 2017). The PMM is positively correlated with TC frequency and strength in the western and eastern north Pacific, sometimes possibly having a dominant effect over ENSO (Gao et al., 2018; Murakami et al., 2017). The PMM has also been linked to increases and decreases in landfalling TCs in the North Atlantic (Zhang et al., 2017). Ongoing research aims to better understand how these modes interact with ENSO and decadal climate modes to impact TCs.

Predictive skill from these interannual climate modes allows for some interannual forecasting of TC seasons. These forecasts can inform energy, resource, and emergency management, as well as insurance pricing, but predictive skill becomes more limited when considering smaller regional scales (Vecchi & Villarini, 2014). Vecchi et al. (2014) provided the first prediction of regional hurricane activity months to seasons in advance; their forecasts used a climate model with 50×50 km atmospheric resolution and gained predictive skill from ENSO and the AMM. Retrospective forecast studies have found substantial impacts of ENSO and the AMM in predicting North Atlantic landfalling TCs (Murakami et al., 2016) and a strong influences of ENSO, the PMM, and potentially decadal variability on TC frequency near Hawaii (Murakami et al., 2015; Murakami et al., 2017). The results suggest that improved forecasting of ENSO would improve long-lead TC forecasts as well. Several studies have also found that hybrid statistical-dynamical models tend to outperform purely statistical or dynamical predictions (e.g., Murakami et al., 2016; Vecchi et al., 2011; Vecchi et al., 2014; Villarini et al., 2019).

However, there are limitations to the predictability of the interannual variability of TCs. Not all teleconnections occur to the same extent during every El Niño and La Niña event. Some ENSO events are stronger than others, and teleconnections can fail during some El Niño events but not others, which can be difficult to predict. Additionally, different TC characteristics have different predictability on the interannual or decadal timescale. Changes in TC tracks and genesis locations have a large weather noise component that limits predictability (Kortum et al., 2024). TC frequency tends to be more predictable, but seasonal predictions are still limited due to the noisiness of the climate system (Vecchi & Villarini, 2014).

It is also important to note that the activity of a TC season does not necessarily correlate with impacts on people. Destructive storms can still occur during less active seasons, and not all active seasons are destructive. For example, the 2010 Atlantic hurricane season was very active, but no hurricanes hit the United States (Beven & Blake, 2015). This is especially important when considering individual locations, such as cities. Predicting destruction due to TCs depends on the TC's path and the environmental conditions that surround it, which tend to be heavily weather-related and therefore predictable on the scale of days or weeks, as well as local risks and exposure which can be anticipated further in advance.

1.7 Tropical cyclone decadal to centennial variability and change

One widely studied subject is the possible influence of human-induced global warming on the decadal to centennial TC variability. Globally, increases in storm intensities and rainfall, a poleward shift in the latitude of maximum intensity, and a slowdown of TC translational speed are potential impending influences of anthropogenic warming on TC activity. However, due to limitations in observations (Yang et al., 2024), it is challenging to confidently attribute such changes to human-induced warming. For example, scientists have limited confidence in TC observations made prior to the start of the satellite era in the 1980s. Without a long, reliable record of storm observations, it remains difficult for scientists to detect long-term trends in storm activity.

In addition to examining past TC records to untangle the relationship between human-induced warming and storm activity, scientists employ computational climate model simulations to project the evolution of storms in a continuously warming world. With medium to high confidence, modeling studies suggest that the proportion of severely intense TCs and the storm precipitation rates will increase. They also project a poleward migration of the latitude of maximum intensity and a slowdown in TC translational speed in select ocean basins.

Knutson et al. (2021)'s review article suggests a consensus among climate scientists that the intensity of storms has increased in the past few decades and that the proportion of global high-intensity storms (Saffir–Simpson Category 4–5) will increase in a future warming world. For instance, Kossin et al. (2020) record an increase in the relative occurrence of storms of Saffir–Simpson Category 3 or higher since the satellite era. Wang et al. (2022) document a 1.8 m s^{-1} per decade increase in weaker storm wind speed from 1991 to 2020. Additionally, in a projected $+2^\circ\text{C}$ warmer world, climate models predict an approximately $+5\%$ increase in the maximum intensity of a storm (Knutson et al., 2020). These results hypothesize an exacerbation of TC-inflicted damage in a warmer world.

Many modeling studies additionally propose that anthropogenic warming is associated with a strengthening of TC rainfall rates, which could aggravate flood risk (Knutson et al., 2015; Kossin, 2018; Liu et al., 2019; Wright et al., 2015). Observed trends in storm rainfall rates, however, do not lie outside a range of possible values governed by natural variability alone. Studies cannot therefore directly link observed changes in TC-induced rainfall to anthropogenic warming.

Several studies (Kossin et al., 2014; Kossin et al., 2016; Staten et al., 2020; Walsh et al., 2019) assess the location where TCs reach their maximum wind speeds. Their results indicate that this latitude of maximum intensity has moved poleward in the past few decades, especially in the Pacific Ocean Basin. These results complement model projections of the locations of storm activity, which predict a poleward shift in the location of maximum intensity in the western North Pacific Ocean in a global warming scenario.

Another uncertainty about TC activity in a warmer world is the evolution of their propagation speed. Although Kossin (2018) and Kossin (2019) observe a slowing of storm translational speed since 1949, these trends are weak and could be limited by observational biases (Lanzante, 2019; Moon et al., 2019). The slowing trend of TCs in the observational record is most robust over the continental United States (Kossin, 2019). In conjunction with these observed trends, Zhang et al. (2020) use models to find that in a warmer world, the TC translational speeds could slow down, especially along the U.S. eastern seaboard. However, this study could not directly attribute a storm slowdown to anthropogenic warming.

One well-researched TC attribute is the evolution of global storm frequencies in a warmer world. Generally, both hindcast observational studies and modeling projection studies agree that there are no clear trends in global TC frequencies since the 1970s (Knutson et al., 2019), and that there are very weak trends in future projections (Knutson et al., 2015). Knutson et al. (2015)'s modeling study finds that there might be a small global negative trend in storm frequencies in a warmer world. However, there is no consensus across modeling studies about the evolution of TC storm frequencies in a late 21st century warmer climate.

There is emerging observational evidence that peak intensities and rapid intensification have changed in recent decades (e.g., Bhatia et al., 2019; Bhatia et al., 2022; Kossin et al., 2020), and future model projections thus agree that anthropogenic warming is associated with an increase in TC intensity. However, the existence and quality of century-scale records of TCs and hurricanes are limited, and largely restricted to the tropical Atlantic at the moment (e.g., Landsea & Franklin, 2013). Even in the tropical Atlantic there is evidence of substantial undersampling of hurricanes in the presatellite era (e.g., Chang & Guo, 2007; Landsea et al., 2010; Mann et al., 2007; Vecchi & Knutson, 2008; Vecchi & Knutson, 2011; Vecchi et al., 2021; Villarini et al., 2011). For example, recorded major hurricane (Category 3–4–5) frequency in the North Atlantic exhibits a clear increase over since the mid-19th century (dashed line in Fig. 1.9). However, when the data is homogenized accounting for known changes in observing practices (blue line in Fig. 1.9), the century-scale increase is less clear and what remains is multidecadal variability and a prominent minimum

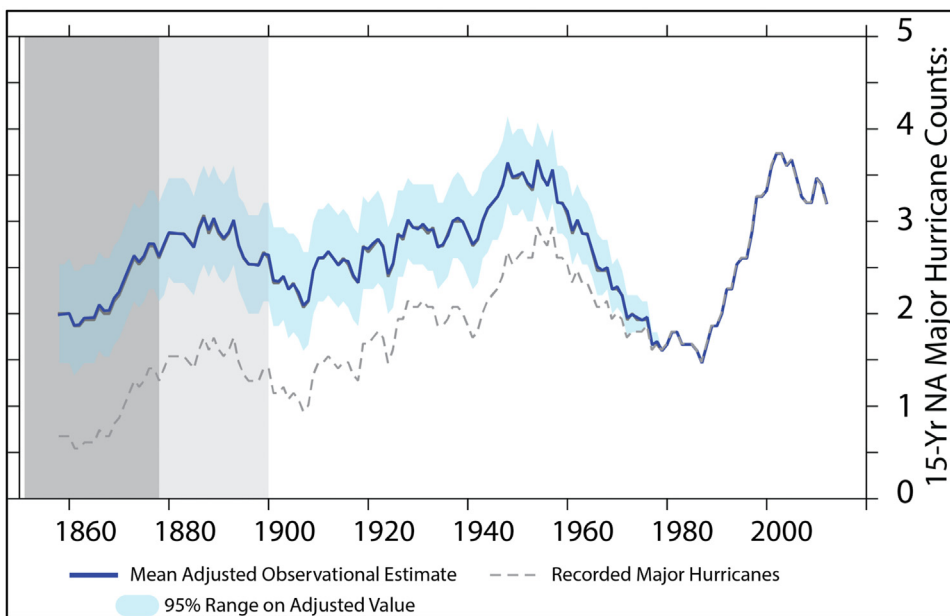


FIGURE 1.9 Fifteen-year running average of North Atlantic major hurricane counts: the raw recorded value (dashed line), the mean adjusted observational estimate (solid line), and the 95% range on the adjusted value. Adapted from Vecchi, G. A., Landsea, C., Zhang, W., Villarini, G., & Knutson, T. (2021). Changes in Atlantic major hurricane frequency since the late-19th century. *Nature Communications*, 12 (1), <http://www.nature.com/ncomms/index.html>. <https://doi.org/10.1038/s41467-021-24268-5>.

in the late 20th century (Vecchi et al., 2021); it has been suggested that this minimum is associated with some combination of internal climate variability and the response to aerosol (particulate pollution) forcing. Chapters 10 and 11 of this book include a deeper discussion of the relationship between TC and climate change.

1.8 Impact of tropical cyclones on climate

TCs have been shown to influence the large-scale climate, with effects modulating both the ocean and the atmosphere.

Regarding impacts on the ocean, local impacts are driven by surface stresses imposed on the air–sea interface by anomalously strong TC winds, leading to localized upwelling and shear-driven vertical mixing. Observational studies have confirmed this among other impacts, with recorded data demonstrating that TCs impact the upper ocean, as areas directly exposed to these storms experience a reduction in SST and a deepening of the oceanic mixed layer (Fisher, 1958; Price, 1981; Stramma et al., 1986). These local effects have been shown to have nonlocal impacts through several pathways. Dynamically, the vertical mixing induced by TCs has been shown to have remote effects through wave propagation (Brizuela et al., 2023; Fandry et al., 1984; Harrison & Giese, 1988), resulting in potential implications for oceanic heat storage (due to advection of subsurface anomalous heat) and upper ocean biology (due to the creation of Kelvin wave–like surges along the eastern coastlines of tropical basins). Thermodynamically, the modification of localized ocean heating implies horizontal advection of heat, resulting in transport of oceanic heat out of areas with TC activity (Emanuel, 2001). Several numerical studies have analyzed this effect using global climate models to show that TC activity may lead to net oceanic poleward heat transport, which has implications for oceanic heat storage and is hypothesized to amplify the atmospheric Hadley circulation due to SST changes (Jansen & Ferrari, 2009; Korty et al., 2008; Scoccimarro et al., 2011; Srivastava & Huber, 2010).

Although the modification to upper ocean properties by TCs appears to impact atmospheric climate, these storms have been shown to directly impact atmospheric moisture and the radiation budget, albeit less robustly than for the oceans. Reanalysis data have been used to show that TCs contribute to localized increases in tropospheric moisture and decreases in outgoing longwave radiation (Camargo & Sobel, 2005), followed by a period of anomalous warming and drying over several months after the TC passage (Emanuel, 2008; Hart et al., 2007). The integration of these local effects over space and time has been linked to modifications to the hydrological cycle and the radiation budget. TCs have been shown to contribute a significant fraction of annual surface freshwater to subtropical regions (Pérez-Alarcón et al., 2023), as well as induce a reduction in precipitation in tropical and subtropical areas not directly impacted by TCs due to a storm-driven moisture transport (Li et al., 2023; Scoccimarro et al., 2020). Additionally, the effects of deep convective clouds associated with these storms have been shown to produce a reduction in net incoming radiation, given the increase in reflected solar radiation due to high cloud cover relative to climatology. However, considerable uncertainty regarding climate-scale impacts of TCs still exists, and remains an area of active investigation.

1.9 Opportunities offered by highly resolved simulations in studying the small-scales properties affecting tropical cyclones intensification

In the last decade, numerical methods capable of directly simulating air-water-wave turbulent processes pertinent to TC microphysics have emerged. Recent advancements in numerical modeling now allow for the full resolution of physics at scales ranging from approximately 100 microns to meters. This includes the detailed behavior of waves, drops, and bubbles in turbulent flows, as well as evaporation processes.

High-fidelity computations of the full three-dimensional breaking wave processes, solving for the native Navier–Stokes equations for coupled air and water flow, with interface reconstruction techniques have become available in the last decade. These high-resolution Direct Numerical Simulations (DNS) mobilize sophisticated tools and computational resources to advance the following challenges: accessing dynamics and statistics spanning multiple scales of fluid behavior that capture interface breaking and reconnection and the associated energetics, bubble and droplets size distribution, all directly coupled to turbulent boundary layers.

These methods rely on breakthroughs in the development of numerical algorithms, allowing to capture surface tension forces accurately while reconstructing the interface via sharp geometric volume of fluid method, and solve for a wide range of scales through adaptive mesh refinement techniques (Popinet, 2009), together with momentum conserving schemes. Convergence of the numerical solutions is probed through grid refinement studies as well as sensitivity to the adaptive mesh algorithm. They provide a path to better understand the complex microphysics of TC conditions.

These techniques have allowed for significant advances in modeling and understanding multiphase turbulent flow, as it allows the full coupling between the air and water phases without any subgrid scale models. The use of adaptive mesh refinement allows it to solve for over three orders of magnitude in spatial scales, therefore probing turbulent processes, as well as drops and bubbles down to an approximate scale of $100\mu\text{m}$ while having a larger wave-scale feature at the meter scale. Fig. 1.10 shows a three-dimensional rendering of a breaking process from the initial steepening to the nonlinear overturning and final breaking.

The principle of adaptive mesh refinement is the following, as discussed in Mostert et al. (2022). The numerical mesh is adaptively refined in order to reduce computational cost. To facilitate such a scheme within a Cartesian grid structure, a tree-based grid is used, which allows nonuniform resolution across the computational domain. The global maximum resolution level is specified by the user and allows for comparison to a fixed grid. The refinement and coarsening scheme itself is based on a wavelet-estimation algorithm. Whether a grid is locally refined or coarsened depends on a choice of the flow variables, on the maximum tolerated errors for these variables. In flows involving interfaces, this leads to high resolution near the interface and within the boundary layers where flow gradients are strong, while deeper in the water (or up in the air), the resolution is coarser. Fig. 1.11 shows an example of this mesh adaptation technique for a wave breaking process. Here, the grid is kept highly refined near the interface and coarse in the far-field region.

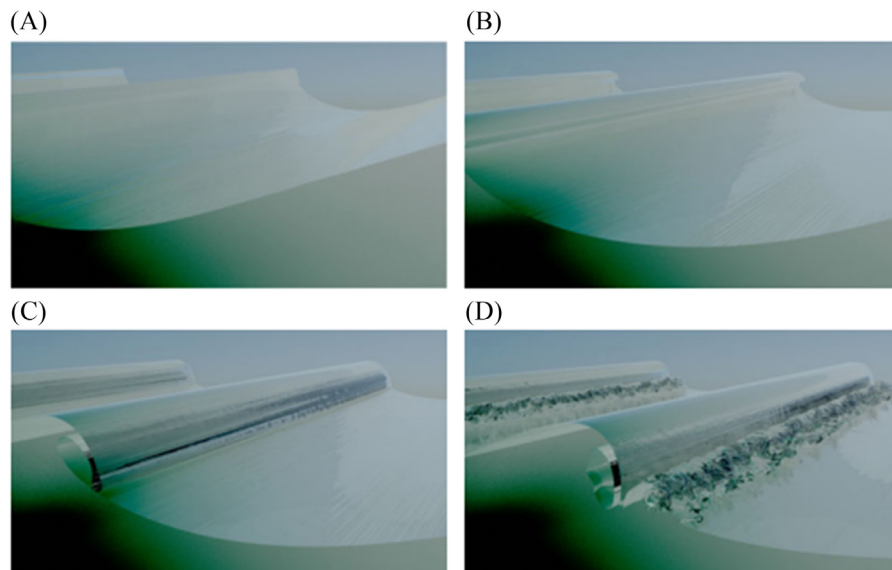


FIGURE 1.10 Renderings of the 3-D breaking wave water–air interface at different times: (A) initial condition, (B) steepening of the wave, (C) nonlinear overturning, and (D) breaking. Taken from Mostert, W., Popinet, S., & Deike, L. (2022). High-resolution direct simulation of deep water breaking waves: Transition to turbulence, bubbles and droplets production. *Journal of Fluid Mechanics*, 942, A27. <https://doi.org/10.1017/jfm.2022.330>.

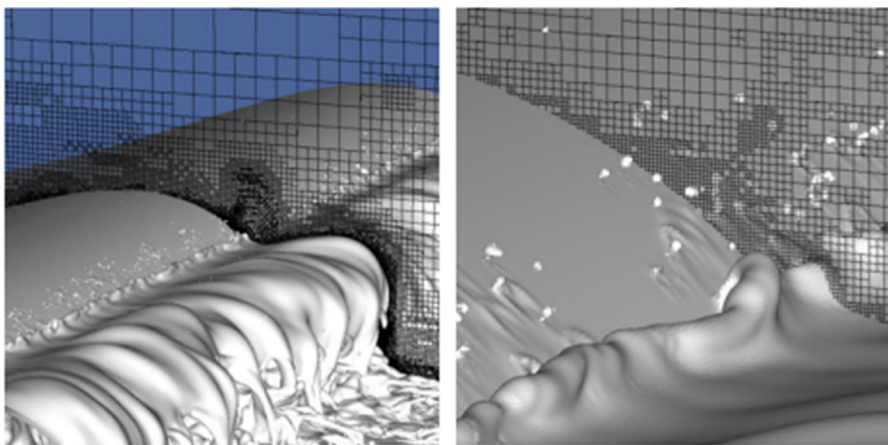


FIGURE 1.11 Renderings of the 3-D breaking wave water-air interface together with the adaptive computational grid at the midplane location of the computational domain. The grid is dynamically refined near the interface and coarse in the far-field region. *Taken from Mostert, W., Popinet, S., & Deike, L. (2022). High-resolution direct simulation of deep water breaking waves: Transition to turbulence, bubbles and droplets production. Journal of Fluid Mechanics, 942, A27. <https://doi.org/10.1017/jfm.2022.330>.*

The physics of breaking waves, including energy dissipation for a wide range of scales and wave slope, was characterized and successfully compared to theoretical inertial turbulence argument, together with an in-depth quantification of air entrainment and bubble size distribution under breaking waves (Deike et al., 2016; Deike, 2022; Mostert et al., 2022). Bubble fragmentation in turbulence was characterized, and data coming from numerical simulations were successfully compared to laboratory experiments (Rivière et al., 2021; Rivière et al., 2022). Simulations of breaking waves allow for direct modeling of sea spray emission during breaking waves (Mostert et al., 2022), a process critical for the understanding of heat transfer at high wind speed.

Simulations solving for the fully coupled turbulent wind and wave growth were also performed and demonstrated the ability of the numerical techniques to accurately capture wind-wave growth up to breaking, including air flow separation (Wu & Deike, 2021; Wu et al., 2022). The simulations highlight the ability to capture the fully coupled air and water side turbulent boundary layer, consisting of a fully developed turbulent air flow interacting with water waves, as shown in Fig. 1.12. They have paved the way for DNS of wind-forced breaking waves in a high-wind speed regime where waves grow under strong wind forcing (high ratio of friction velocity over wave speed), develop, and eventually break. Following breaking, the waves grow again. These simulations can then be used to analyze the momentum and energy fluxes budgets during the growing and breaking stages. The momentum budget shows a sudden reduction during the breaking stage that can be associated with strong air flow separation. At high ratios of wind friction velocity to wave speed, the increase in pressure drag is balanced by the reduction during breaking, leading to a saturation of the pressure drag coefficient over an entire breaking cycle. The reduction in the pressure drag at high wind speeds is also confirmed by inspecting the streamwise velocity profile, which shifts to larger values at the breaking stage. These simulations recover drag coefficient saturation at high wind speeds. Analysis of the energy budget reveals that the breaking process and injection of kinetic energy by the wave is largely independent of the wind forcing above, and that scalings developed for breaking waves in the absence of wind describe well the energy loss by the wave during the breaking stage.

1.9.1 Mass exchange: gas, evaporation, single bubble/drop, or collective effect in turbulence

The continuous development in numerical algorithms and in the computational power has recently enabled highly resolved simulations of multiphase flows, incorporating fully coupled mass, momentum, and heat transfer processes. These simulations are applicable to various environmental flows, such as those involving bubbles and droplets generated following wave breaking events. Bubbles result from the significant amount of gas entrained in the water currents, as discussed in Deike et al. (2015) and Deane and Stokes (1999). Droplets form as sea sprays, which have several sources. The primary source is wave breaking itself, due to the local rupture of the ocean surface (Veron, 2015). Another source is bubble bursting, which occurs when bubbles entrained in the water currents rise to the ocean surface and release liquid droplets into the atmosphere (Veron, 2015). Bubbles and droplets, through dissolution and evaporation processes, respectively, play crucial roles in mediating the mass, momentum, and energy exchanges at the ocean–atmosphere interface. For example, bubble entrainment is estimated to mediate around 40% of the gas exchanges, such as oxygen and carbon dioxide, between the ocean and the atmosphere (Deike, 2022). Therefore accurately predicting their dissolution and evaporation rates is of critical importance.

1.9.2 Bubbles dissolution

Bubble dissolution is a phase-change mechanism involving the coupled transport of mass and momentum. This process is often isothermal, allowing the temperature influence to be neglected.

A priori estimations of the dissolution rate or its dimensionless definition, the Sherwood number, are particularly valuable in turbulent configurations. Turbulence is known to enhance the dissolution rate, but quantifying its effect across different turbulence levels, characterized by the Reynolds number, and gas diffusivity, characterized by the Schmidt number, is not straightforward. To address this gap, Farsoiya et al. (2021) developed a numerical algorithm to study mass transfer in gas bubbles under dilute conditions, applying it to compute the Sherwood number of a single bubble in homogeneous and isotropic turbulence (HIT), as the one reported in Fig. 1.13. The HIT setup allows for precise, isolated testing of turbulence's effect on the dissolution rate. The dilute assumption was later relaxed in Farsoiya et al. (2023), where the same authors extended the Sherwood number correlation to higher Reynolds numbers, suggesting that the dissolution rate for bubbles could be predicted for arbitrary levels of turbulence. The applicability of these numerical algorithms to gas bubbles resulting from wave breaking, as shown in Fig. 1.14, was demonstrated in Farsoiya et al. (2022).

1.9.3 Droplets and films evaporation

Droplet evaporation involves heat exchange through latent heat, which is a significant contribution to energy transfer in environmental applications involving water droplets. Unlike bubble dissolution, evaporation cannot be approximated as an isothermal process and the temperature at which the process occurs greatly influences the process. Numerical algorithms have been developed to study droplet evaporation in turbulent flows (Cipriano et al., 2024; Scapin et al., 2020), accounting for the simultaneous transfer of mass, momentum, and energy. These algorithms have been applied to study isolated droplets in HIT (Dodd et al., 2021) and in homogeneous shear turbulence (Scapin, 2022) to test the robustness of the d^2 law, which states that the square of an isolated evaporating droplet's diameter decreases linearly with time.

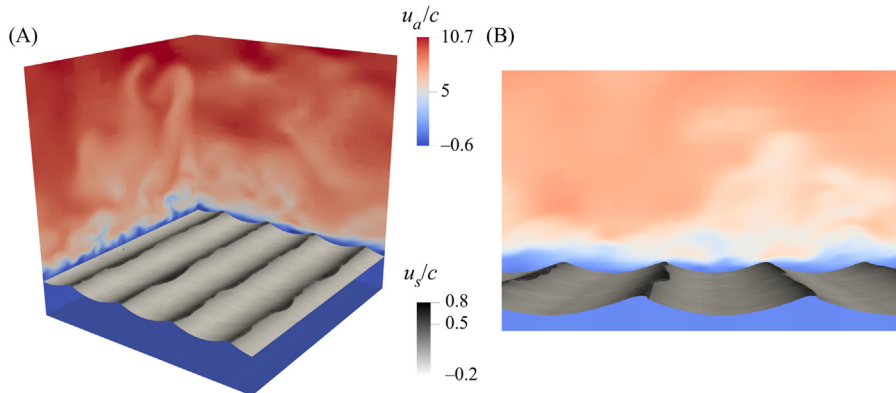


FIGURE 1.12 Wind-forced growing waves at incipient breaking in a two-phase turbulent boundary layer. The two color bars indicate the horizontal wind velocity (normalized by the friction velocity) and the surface water velocity (normalized by the wave speed). Taken from Wu, J., Popinet, S., & Deike, L. (2022). Revisiting wind wave growth with fully coupled direct numerical simulations. Journal of Fluid Mechanics, 951, A18. <https://doi.org/10.1017/jfm.2022.822>.

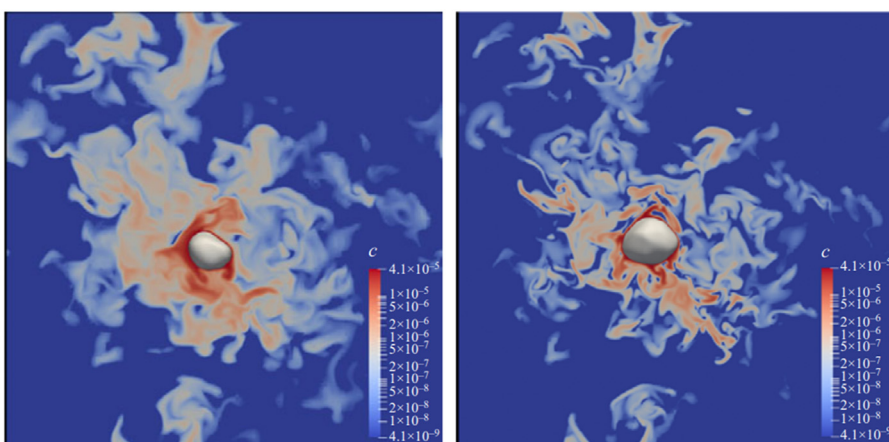


FIGURE 1.13 Bubbles dissolving in turbulence at two values of gas diffusivity (high value on the left panel, low value on the right panel). The color bar shows the contour of CO₂ concentration. Taken from Farsoiya, P. K., Magdelaine, Q., Antkowiak, A., Popinet, S., & Deike, L. (2023). Direct numerical simulations of bubble-mediated gas transfer and dissolution in quiescent and turbulent flows. Journal of Fluid Mechanics, 954. <http://journals.cambridge.org/action/displayJournal?jid=FLM>. <https://doi.org/10.1017/jfm.2022.994>.

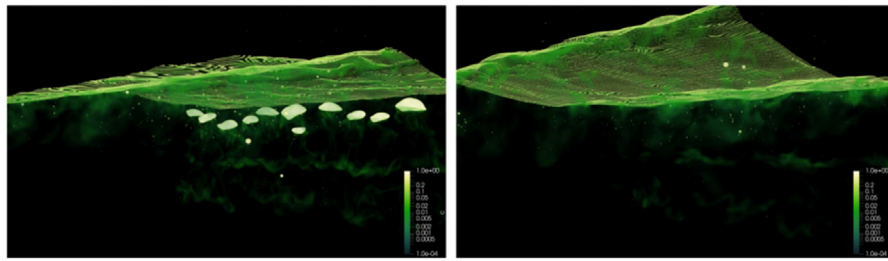


FIGURE 1.14 Gas bubbles dissolving in turbulent water currents at two values of gas diffusivity (high value on the left panel, low value on the right panel). The gas bubbles are formed following wave breaking events due to air entrainment. The color bar shows the contour of CO_2 concentration. Taken from Farsoiya, P. K., Popinet, S., & Deike, L. (2022). Direct numerical simulations of dilute gas transfer by breaking waves. *Physical Review Fluids* 7 (11). <https://journals.aps.org/prfluids/abstract/10.1103/PhysRevFluids.7.110506>. <https://doi.org/10.1103/PhysRevFluids.7.110506>.

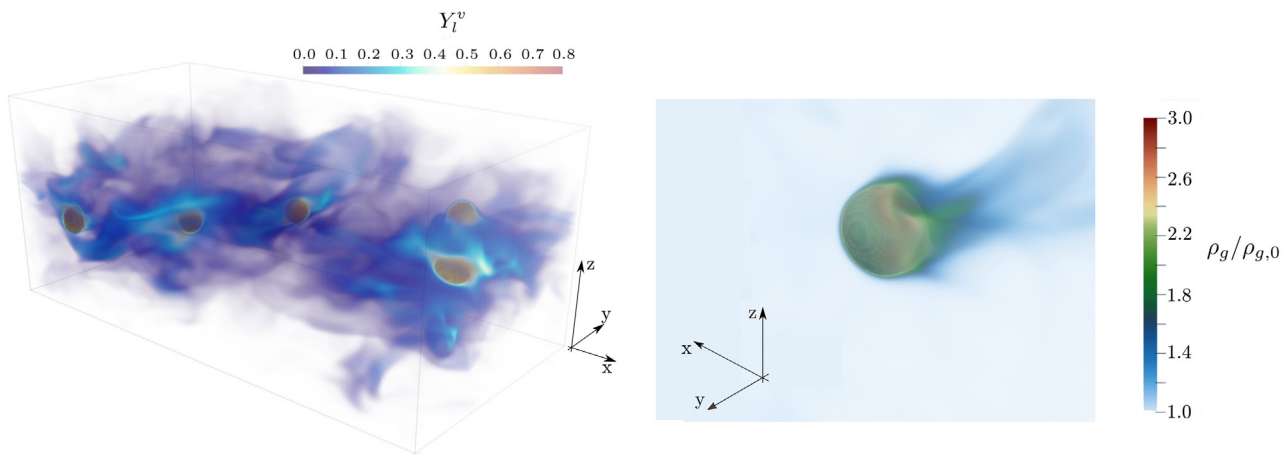


FIGURE 1.15 Evaporating droplets in homogeneous shear turbulence. The left panel includes the volume rendering of the vapor clouds around the droplets. Note that the vapor concentration is much larger at the droplet position and drastically reduces in the far-field region. The right panel includes the gas density field around a single droplet. At high temperature, the gas density around the droplet can be up to three times larger than the one in the far field region due to the cooling effect induced by evaporation. Taken from Scapin, N. (2022). Phase-changing flows: Numerical methods and fully resolved simulations [Dissertation, KTH Royal Institute of Technology].

Fig. 1.15 shows three-dimensional renderings of evaporating droplets in turbulence. These studies also compute the Sherwood number for different Reynolds numbers and gas temperatures. Notably, the linear regime of the d^2 law has been observed even at large volume fractions (Dodd et al., 2021; Scapin, 2022). Additional fully resolved simulations of evaporation have been applied to study phase-changing flows in multiphase thermal convection (Scapin et al., 2023), where evaporation occurs at a flat gas–liquid interface and alters the transport properties by modifying the local thermophysical properties. Scaling laws for the heat transfer modulation and interface temperature can be derived and extrapolated to higher turbulence levels.

1.9.4 Perspectives on phase-changing studies for studying tropical cyclones

At sufficiently high wind speeds, that is, greater than $30\text{--}35 \text{ m s}^{-1}$, the ocean surface is dominated by wave breaking, producing a large amount of droplets. The increased surface area (per unit volume) compared to a flat surface significantly enhances heat and mass transfer processes, impacting the energy budget of the atmospheric boundary layer (Veron, 2015; Sroka & Emmanuel, 2021). Precisely estimating these fluxes is crucial for understanding the physics of TC intensification and maximum storm intensities. A common approach to parameterize the energy exchanges is by introducing the enthalpy bulk coefficient. This quantity remains constant up to 20 m s^{-1} , with a sharp increase at wind speeds greater than 25 m s^{-1} . This significant rise is attributed to the presence of sea spray, which greatly enhances air-sea enthalpy fluxes. Highly resolved simulations have been employed to study the transport of sea spray in the atmospheric boundary layer using the point-particle (PP) approach, treating droplets as massless points and incorporating correlations to estimate their evaporation rate (Peng & Richter, 2019; Richter & Wainwright, 2023). Despite their

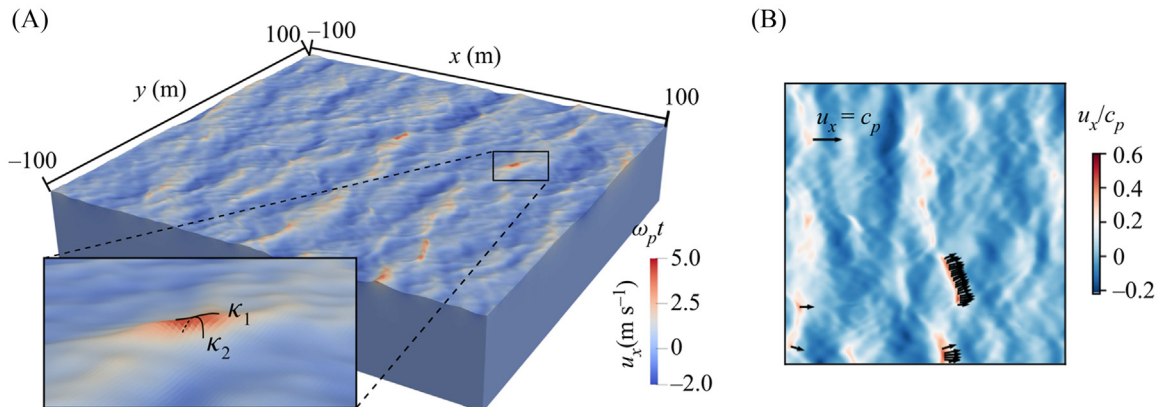


FIGURE 1.16 Breaking wave field simulated with a multilayer framework. The left panel represents the three-dimensional rendering of the breaking wave field with the color indicating the surface layer flow velocity. Inset shows the curvature of the breaking fronts as the detection criterion. The right panel is the top view of the breaking field with different breaking fronts (black arrows). Taken from Wu, J., Popinet, S., & Deike, L. (2023). *Breaking wave field statistics with a multi-layer model*. Journal of Fluid Mechanics, 968, A12. <https://doi.org/10.1017/jfm.2023.522>.

widespread use, the PP approach cannot reproduce important effects that can potentially affect the air-sea fluxes: turbulence modulation induced by the droplets, coalescence and breakup, and deviations from the d^2 law due to collective behavior. Alternatively, these effects can be captured by relaxing the PP approach and performing interface-resolved simulations of the evaporation process.

1.9.5 Bridging the scales

While the abovementioned methods provide a path to better understand detailed microphysics relevant to high turbulent two-phase flows, an intermediate set of numerical methods are required to bridge with large-scale models able to resolve TCs at scale.

Large Eddy Simulation (LES) has been a preferred method when studying intermediate-scale wind–wave interaction ($O(1\text{ m})$ – $O(1\text{ km})$) since it only resolves large scale, dynamically important eddies in turbulence, and is therefore computationally more effective (Sullivan et al., 2008). The challenge lies in including the small-scale effect within subgrid scale modeling, in this case the representation of waves and drops and their interaction with turbulence below the grid resolution, together with complex treatment of the coupling between the two phases, implicitly assuming accurate knowledge of the momentum flux into small-scale waves. However, such processes remain poorly understood, making the LES subgrid models part of the uncertainties, with the presence of sea spray and its role on enthalpy fluxes adding another layer of complexity since it requires knowledge of the droplets size and velocity source function (Barr et al., 2023; Richter & Wainwright, 2023).

A recent modeling framework can lead to a better representation of wind–wave–ocean coupling at these intermediate scales, fully resolving broad-banded wave spectra including breaking waves. A multilayer framework developed by Popinet (2020) allows to resolve a patch of breaking waves at scales $O(1\text{ m}$ – 1 km) as demonstrated by Wu et al. (2023). The multilayer framework generalizes the single-layer Saint-Venant system into a multilayer and nonhydrostatic formulation of the Navier–Stokes equations. The novel algorithm allows to simulate an ensemble of broad-banded surface wave fields in the physical space, including directional wave breaking and the associated turbulent flow. Wu et al. (2023) demonstrate excellent agreement of the kinematics of wave breaking by identifying breaking fronts and their speed, and are found to be in good agreement with field measurements. Fig. 1.16 shows a three-dimensional rendering of the breaking field simulated with the multilayer framework. Investigation of air–flow coupling with a wave spectra representative of TC conditions would be a natural extension of this work. Each breaking event could then be associated with spray generation, heat, and momentum exchange modeled in a way consistent with the knowledge gained in the high-fidelity DNS (Figs. 1.13–1.16).

References

- Anthes, R. A. (1974). The dynamics and energetics of mature tropical cyclones. *Reviews of Geophysics*, 12(3). Available from <https://doi.org/10.1029/RG012i003p00495>.

- Barr, B. W., Chen, S. S., & Fairall, C. W. (2023). Sea-state-dependent sea spray and air–sea heat fluxes in tropical cyclones: A new parameterization for fully coupled atmosphere–wave–ocean models. *Journal of the Atmospheric Sciences*, 80, 933–960. Available from <https://doi.org/10.1175/JAS-D-22-0126.1>.
- Bell, G. D., Michael, S., Halpert, R. C., Wayne Schnell, R., Higgins, J., Lawrimore, V. E., Kousky, R., Tinker, W., Thiaw., Chelliah, M., & Artusa, A. (2000). Climate assessment for 1999. *Bulletin of the American Meteorological Society*, 81. Available from [https://doi.org/10.1175/1520-0477\(2000\)81](https://doi.org/10.1175/1520-0477(2000)81).
- Beven, J. L., & Blake, E. S. (2015). Atlantic hurricane season of 2010. *Monthly Weather Review*, 143(9). Available from <https://doi.org/10.1175/MWR-D-11-00264.1>, <http://journals.ametsoc.org/doi/pdf/10.1175/MWR-D-11-00264.1>.
- Bhatia, K., Baker, A., Yang, W., Vecchi, G., Knutson, T., Murakami, H., Kossin, J., Hodges, K., Dixon, K., Bronselaer, B., & Whitlock, C. (2022). A potential explanation for the global increase in tropical cyclone rapid intensification. *Nature Communications*, 13(1). Available from <https://doi.org/10.1038/s41467-022-34321-6>.
- Bhatia, K. T., Vecchi, G. A., Knutson, T. R., Murakami, H., Kossin, J., Dixon, K. W., & Whitlock, C. E. (2019). Recent increases in tropical cyclone intensification rates. *Nature Communications*, 10(1). Available from <https://doi.org/10.1038/s41467-019-08471-z>.
- Bister, M., & Emanuel, K. A. (1998). Dissipative heating and hurricane intensity. *Meteorology and Atmospheric Physics*, 65(3–4). Available from <https://doi.org/10.1007/bf01030791>.
- Brizuela, N. G., Alford, M. H., Xie, S. P., Sprintall, J., Voet, G., Warner, S. J., Hughes, K., & Moum, J. N. (2023). Prolonged thermocline warming by near-inertial internal waves in the wakes of tropical cyclones. *Proceedings of the National Academy of Sciences of the United States of America*, 120(26). Available from <https://doi.org/10.1073/pnas.2301664120>, <https://www.pnas.org/doi/epdf/10.1073/pnas.2301664120>.
- Camargo, S. J., Camp, J., Elsberry, R. L., Gregory, P. A., Klotzbach, P. J., Schreck, C. J., Sobel, A. H., Ventrice, M. J., Vitart, F., Wang, Z., Wheeler, M. C., Yamaguchi, M., & Zhan, R. (2019). Tropical cyclone prediction on subseasonal time-scales. *Tropical Cyclone Research and Review*, 8(3). Available from <https://doi.org/10.1016/j.tccr.2019.10.004>.
- Camargo, S. J., & Sobel, A. H. (2005). Western North Pacific tropical cyclone intensity and ENSO. *Journal of Climate*, 18(15), 2996–3006. Available from <https://doi.org/10.1175/JCLI3457.1>.
- Cannon, G. H., & Kaye, A. S. (1994). *The Arabic contributions to the English language: An historical dictionary*. Otto Harrassowitz Verlag.
- Chan, J. C. L. (1985). Tropical cyclone activity in the northwest Pacific in relation to the El Niño/Southern Oscillation phenomenon. *Monthly Weather Review*, 113(4). Available from [https://doi.org/10.1175/1520-0493\(1985\)113<0599:TCAITN>2.0.CO;2](https://doi.org/10.1175/1520-0493(1985)113<0599:TCAITN>2.0.CO;2).
- Chan, J. C. L. (2005a). The physics of tropical cyclone motion. *Annual Review of Fluid Mechanics*, 37, 99–128. Available from <https://doi.org/10.1146/annurev.fluid.37.061903.175702>.
- Chan, J. C. L. (2005b). Interannual and interdecadal variations of tropical cyclone activity over the western North Pacific. *Meteorology and Atmospheric Physics*, 89(1–4). Available from <https://doi.org/10.1007/s00703-005-0126-y>.
- Chand, S. S., Walsh, K. J. E., Camargo, S. J., Kossin, J. P., Tory, K. J., Wehner, M. F., Chan, J. C. L., Klotzbach, P. J., Dowdy, A. J., Bell, S. S., Ramsay, H. A., & Murakami, H. (2022). Declining tropical cyclone frequency under global warming. *Nature Climate Change*, 12(7). Available from <https://doi.org/10.1038/s41558-022-01388-4>, <http://www.nature.com/nclimate/index.html>.
- Chang, E. K. M., & Guo, Y. (2007). Is the number of North Atlantic tropical cyclones significantly underestimated prior to the availability of satellite observations? *Geophysical Research Letters*, 34(14). Available from <https://doi.org/10.1029/2007GL030169>.
- Chatterjee, P., & Goswami, B. N. (2004). Structure, genesis and scale selection of the tropical quasi-biweekly mode. *Quarterly Journal of the Royal Meteorological Society*, 130(559). Available from <https://doi.org/10.1256/qj.03.133>.
- Cipriano, E., Saufi, A. E., Frassoldati, A., Faravelli, T., Popinet, S., & Cuoci, A. (2024). Multicomponent droplet evaporation in a geometric volume-of-fluid framework. *Journal of Computational Physics*, 507. Available from <https://doi.org/10.1016/j.jcp.2024.112955>, <https://www.sciencedirect.com/science/journal/00219991>.
- Colle, B. A. (2003). Numerical simulations of the extratropical transition of Floyd (1999): Structural evolution and responsible mechanisms for the heavy rainfall over the Northeast United States. *Monthly Weather Review*, 131(12). Available from [https://doi.org/10.1175/1520-0493\(2003\)131<2905:NSOTET>2.0.CO;2](https://doi.org/10.1175/1520-0493(2003)131<2905:NSOTET>2.0.CO;2).
- Deane, G. B., & Stokes, M. D. (1999). Air entrainment processes and bubble size distributions in the surf zone. *Journal of Physical Oceanography*, 29 (7). Available from <http://journals.ametsoc.org/loi/phoc>, [https://doi.org/10.1175/1520-0485\(1999\)029<1393:AEPABS>2.0.CO;2](https://doi.org/10.1175/1520-0485(1999)029<1393:AEPABS>2.0.CO;2).
- Deike, L. (2022). Mass transfer at the ocean–atmosphere interface: The role of wave breaking, droplets, and bubbles. *Annual Review of Fluid Mechanics*, 54(1). Available from <https://doi.org/10.1146/annurev-fluid-030121-014132>.
- Deike, L., Melville, W. K., & Popinet, S. (2016). Air entrainment and bubble statistics in breaking waves. *Journal of Fluid Mechanics*, 801, 91–129. Available from <https://doi.org/10.1017/jfm.2016.372>.
- Deike, L., Popinet, S., & Melville, W. K. (2015). Capillary effects on wave breaking. *Journal of Fluid Mechanics*, 769, 541–569. Available from <https://doi.org/10.1017/jfm.2015.103>.
- Dodd, M. S., Mohaddes, D., Ferrante, A., & Ihme, M. (2021). Analysis of droplet evaporation in isotropic turbulence through droplet-resolved DNS. *International Journal of Heat and Mass Transfer*, 172, 121157. Available from <https://doi.org/10.1016/j.ijheatmasstransfer.2021.121157>.
- Dowdy, A. J., Qi, L., Jones, D., Ramsay, H., Fawcett, R., & Kuleshov, Y. (2012). Tropical cyclone climatology of the south pacific ocean and its relationship to El Niño-Southern oscillation. *Journal of Climate*, 25(18). Available from <https://doi.org/10.1175/JCLI-D-11-00647.1>, <http://journals.ametsoc.org/doi/pdf/10.1175/JCLI-D-11-00647.1>.
- Emanuel, K. (2001). Contribution of tropical cyclones to meridional heat transport by the oceans. *Journal of Geophysical Research: Atmospheres*, 106 (D14). Available from <https://doi.org/10.1029/2000jd900641>.

- Emanuel, K. (2005). Increasing destructiveness of tropical cyclones over the past 30 years. *Nature*, 436(7051), 686–688. Available from <https://doi.org/10.1038/nature03906>.
- Emanuel, K. (2007). Environmental factors affecting tropical cyclone power dissipation. *Journal of Climate*, 20(22), 5497–5509. Available from <https://doi.org/10.1175/2007JCLI1571.1>.
- Emanuel, K. (2008). The hurricane-climate connection. *Bulletin of the American Meteorological Society*, 89(5), ES10. Available from <https://doi.org/10.1175/BAMS-89-5-Emanuel>, <http://ams.allenpress.com/archive/1520-0477/89/5/pdf/i1520-0477-89-5-ES10.pdf>, United States.
- Emanuel, K. (2022). Tropical cyclone seeds, transition probabilities, and genesis. *Journal of Climate*, 35(11). Available from <https://doi.org/10.1175/JCLI-D-21-0922.1>, <https://journals.ametsoc.org/view/journals/clim/35/11/JCLI-D-21-0922.1.xml>.
- Emanuel, K., & Nolan, D. S. (2004). Tropical cyclone activity and the global climate system. In *26th conference on hurricanes and tropical meteorology* (pp. 240–241). United States.
- Emanuel, K. A. (1995). Sensitivity of tropical cyclones to surface exchange coefficients and a revised steady-state model incorporating eye dynamics. *Journal of the Atmospheric Sciences*, 52, 3969–3976. Available from [https://doi.org/10.1175/1520-0469\(1995\)052<3969:SOTCTS>2.0.CO;2](https://doi.org/10.1175/1520-0469(1995)052<3969:SOTCTS>2.0.CO;2).
- Emanuel, K. A. (1986). An air-sea interaction theory for tropical cyclones. Part I: Steady-state maintenance. *Journal of the Atmospheric Sciences*, 43(6). Available from [https://doi.org/10.1175/1520-0469\(1986\)043<0585:aasitf>2.0.co;2](https://doi.org/10.1175/1520-0469(1986)043<0585:aasitf>2.0.co;2).
- Fandry, C. B., Leslie, L. M., & Steedman, R. K. (1984). Kelvin-type coastal surges generated by tropical cyclones. *Journal of Physical Oceanography*, 14, 582–593. Available from [https://doi.org/10.1175/1520-0485\(1984\)014<0582:KTCSGB>2.0.CO;2](https://doi.org/10.1175/1520-0485(1984)014<0582:KTCSGB>2.0.CO;2).
- Farsoiya, P. K., Magdelaine, Q., Antkowiak, A., Popinet, S., & Deike, L. (2023). Direct numerical simulations of bubble-mediated gas transfer and dissolution in quiescent and turbulent flows. *Journal of Fluid Mechanics*, 954. Available from <https://doi.org/10.1017/jfm.2022.994>, <http://journals.cambridge.org/action/displayJournal?jid=FLM>.
- Farsoiya, P. K., Popinet, S., & Deike, L. (2021). Bubble-mediated transfer of dilute gas in turbulence. *Journal of Fluid Mechanics*, 920, A34. Available from <https://doi.org/10.1017/jfm.2021.447>.
- Farsoiya, P. K., Popinet, S., & Deike, L. (2022). Direct numerical simulations of dilute gas transfer by breaking waves. *Physical Review Fluids*, 7(11). Available from <https://doi.org/10.1103/PhysRevFluids.7.110506>, <https://journals.aps.org/prfluids/abstract/10.1103/PhysRevFluids.7.110506>.
- Fisher, E. L. (1958). Hurricanes and the sea-surface temperature field. *Journal of Meteorology*, 15(3). Available from [https://doi.org/10.1175/1520-0469\(1958\)015<0328:hatsst>2.0.co;2](https://doi.org/10.1175/1520-0469(1958)015<0328:hatsst>2.0.co;2).
- Fowler, M. D., & Pritchard, M. S. (2020). Regional MJO modulation of Northwest Pacific tropical cyclones driven by multiple transient controls. *Geophysical Research Letters*, 47(11). Available from <https://doi.org/10.1029/2020gl087148>.
- Frank, W. M., & Young, G. S. (2007). The interannual variability of tropical cyclones. *Monthly Weather Review*, 135(10). Available from <https://doi.org/10.1175/MWR3435.1>.
- Gao, S., Zhu, L., Zhang, W., & Chen, Z. (2018). Strong modulation of the Pacific meridional mode on the occurrence of intense tropical cyclones over the Western North Pacific. *Journal of Climate*, 31(19). Available from <https://doi.org/10.1175/jcli-d-17-0833.1>.
- Gray, W. M. (1979). *Hurricanes: Their formation, structure and likely role in the tropical circulation. Meteorology over the tropical oceans*. Royal Meteorological Society.
- Gray, W. M. (1984). Atlantic seasonal hurricane frequency. Part I: El Niño and 30 mb quasi-biennial oscillation influences. *Monthly Weather Review*, 112(9). Available from [https://doi.org/10.1175/1520-0493\(1984\)112<1649:ashfpi>2.0.co;2](https://doi.org/10.1175/1520-0493(1984)112<1649:ashfpi>2.0.co;2).
- Gray, W. M. (May 26, 1988). *Forecast of Atlantic seasonal hurricane activity for 1988* (Report, pp. 13–14). Colorado State University.
- Harris, L., Zhou, L., Lin, S. J., Chen, J. H., Chen, X., Gao, K., Morin, M., Rees, S., Sun, Y., Tong, M., Xiang, B., Bender, M., Benson, R., Cheng, K. Y., Clark, S., Elbert, O. D., Hazelton, A., Huff, J. J., Kaltenbaugh, A., . . . Stern, W. (2020). GFDL SHIELD: A unified system for weather-to-seasonal prediction. *Journal of Advances in Modeling Earth Systems*, 12(10). Available from <https://doi.org/10.1029/2020MS002223>, [http://agu-pubs.onlinelibrary.wiley.com/agu/journal/10.1002/\(ISSN\)1942-2466/](http://agu-pubs.onlinelibrary.wiley.com/agu/journal/10.1002/(ISSN)1942-2466/).
- Harrison, D. E., & Giese, B. S. (1988). Remote westerly wind forcing of the eastern equatorial Pacific; some model results. *Geophysical Research Letters*, 15(8). Available from <https://doi.org/10.1029/gl015i008p00804>.
- Hart, R. E., Maue, R. N., & Watson, M. C. (2007). Estimating local memory of tropical cyclones through MPI anomaly evolution. *Monthly Weather Review*, 135, 3990–4005. Available from <https://doi.org/10.1175/2007MWR2038.1>.
- Holland, G. J. (1997). The maximum potential intensity of tropical cyclones. *Journal of the Atmospheric Sciences*, 54(21). Available from <http://journals.ametsoc.org/loi/atsc>, [https://doi.org/10.1175/1520-0469\(1997\)054<2519:TMPIOT>2.0.CO;2](https://doi.org/10.1175/1520-0469(1997)054<2519:TMPIOT>2.0.CO;2).
- Hsieh, T. L., Vecchi, G. A., Yang, W., Held, I. M., & Garner, S. T. (2020). Large-scale control on the frequency of tropical cyclones and seeds: A consistent relationship across a hierarchy of global atmospheric models. *Climate Dynamics*, 55(11–12). Available from <https://doi.org/10.1007/s00382-020-05446-5>, <http://link.springer.de/link/service/journals/00382/index.htm>.
- Hsieh, T. L., Yang, W., Vecchi, G. A., & Zhao, M. (2022). Model spread in the tropical cyclone frequency and seed propensity index across global warming and ENSO-like perturbations. *Geophysical Research Letters*, 49(7). Available from <https://doi.org/10.1029/2021GL097157>, [http://agu-pubs.onlinelibrary.wiley.com/hub/journal/10.1002/\(ISSN\)1944-8007/](http://agu-pubs.onlinelibrary.wiley.com/hub/journal/10.1002/(ISSN)1944-8007/).
- Hsieh, T. L., Zhang, B., Yang, W., Vecchi, G. A., Zhao, M., Soden, B. J., & Wang, C. (2023). The influence of large-scale radiation anomalies on tropical cyclone frequency. *Journal of Climate*, 36(16). Available from <https://doi.org/10.1175/JCLI-D-22-0449.1>, <https://journals.ametsoc.org/view/journals/clim/36/16/JCLI-D-22-0449.1.xml>.
- Irish, J. L., Resio, D. T., & Ratcliff, J. J. (2008). The influence of storm size on hurricane surge. *Journal of Physical Oceanography*, 38(9), 2003–2013. Available from <https://doi.org/10.1175/2008JPO3727.1>.

- Jansen, M., & Ferrari, R. (2009). Impact of the latitudinal distribution of tropical cyclones on ocean heat transport. *Geophysical Research Letters*, 36(6). Available from <https://doi.org/10.1029/2008GL036796>.
- Jones, S. C., Harr, P. A., Abraham, J., Bosart, L. F., Bowyer, P. J., Evans, J. L., Hanley, D. E., Hanstrum, B. N., Hart, R. E., Lalaurette, F., Sinclair, M. R., Smith, R. K., & Thorncroft, C. (2003). The extratropical transition of tropical cyclones: Forecast challenges, current understanding, and future directions. *Weather and Forecasting*, 18(6). Available from [https://doi.org/10.1175/1520-0434\(2003\)018<1052:TETOTC>2.0.CO;2](https://doi.org/10.1175/1520-0434(2003)018<1052:TETOTC>2.0.CO;2).
- Kikuchi, K. (2021). The Boreal Summer Intraseasonal Oscillation (BSISO): A review. *Journal of the Meteorological Society of Japan. Ser. II*, 99(4). Available from <https://doi.org/10.2151/jmsj.2021-045>.
- Klein, P. M., Harr, P. A., & Elsberry, R. L. (2000). Extratropical transition of Western North Pacific tropical cyclones: An overview and conceptual model of the transformation stage. *Weather and Forecasting*, 15, 373–395. Available from [https://doi.org/10.1175/1520-0434\(2000\)015<0373:ETONP>2.0.CO;2](https://doi.org/10.1175/1520-0434(2000)015<0373:ETONP>2.0.CO;2).
- Klotzbach, P. J., Bell, M. M., Bowen, S. G., Gibney, E. J., Knapp, K. R., & Schreck, C. J. (2020). Surface pressure a more skillful predictor of normalized hurricane damage than maximum sustained wind. *Bulletin of the American Meteorological Society*, 101(6), E830. Available from <https://doi.org/10.1175/bams-d-19-0062.1>.
- Klotzbach, P. J., & Oliver, E. C. J. (2015). Modulation of Atlantic basin tropical cyclone activity by the Madden-Julian oscillation (MJO) from 1905 to 2011. *Journal of Climate*, 28(1). Available from <https://doi.org/10.1175/JCLI-D-14-00509.1>, <http://journals.ametsoc.org/doi/pdf/10.1175/JCLI-D-14-00509.1>.
- Knutson, T., Camargo, S. J., Chan, J. C. L., Emanuel, K., Ho, C.-H., Kossin, J., Mohapatra, M., Satoh, M., Sugi, M., Walsh, K., & Wu, L. (2020). Tropical cyclones and climate change assessment: Part II: Projected response to anthropogenic warming. *Bulletin of the American Meteorological Society*, 101(3), E303. Available from <https://doi.org/10.1175/bams-d-18-0194.1>.
- Knutson, T., Camargo, S. J., Chan, J. C. L., Emanuel, K., Ho, C.-H., Kossin, J., Mohapatra, M., Satoh, M., Sugi, M., Walsh, K., & Wu, L. (2019). Tropical cyclones and climate change assessment: Part I: Detection and attribution. *Bulletin of the American Meteorological Society*, 100(10). Available from <https://doi.org/10.1175/bams-d-18-0189.1>.
- Knutson, T. R., Chung, M. V., Vecchi, G., Sun, J., Hsieh, T.-L., & Smith, A. J. P. (2021). Climate change is probably increasing the intensity of tropical cyclones. In C. Le Quéré, P. Liss, & P. Foster (Eds.), *ScienceBrief Review (Critical issues in climate change science series)*.
- Knutson, T. R., Sirutis, J. J., Zhao, M., Tuleya, R. E., Bender, M., Vecchi, G. A., Villarini, G., & Chavas, D. (2015). Global projections of intense tropical cyclone activity for the late twenty-first century from dynamical downscaling of CMIP5/RCP4.5 scenarios. *Journal of Climate*, 28(18). Available from <https://doi.org/10.1175/jcli-d-15-0129.1>.
- Kortum, G., Vecchi, G. A., Hsieh, T. L., & Yang, W. (2024). Influence of weather and climate on multidecadal trends in Atlantic hurricane genesis and tracks. *Journal of Climate*, 37(5). Available from <https://doi.org/10.1175/JCLI-D-23-0088.1>, <https://journals.ametsoc.org/view/journals/clim/37/5/JCLI-D-23-0088.1.xml>.
- Korty, R. L., Emanuel, K. A., & Scott, J. R. (2008). Tropical cyclone-induced upper-ocean mixing and climate: Application to equable climates. *Journal of Climate*, 21, 638–654. Available from <https://doi.org/10.1175/2007JCLI1659.1>.
- Kossin, J. P. (2018). A global slowdown of tropical-cyclone translation speed. *Nature*, 558(7708). Available from <https://doi.org/10.1038/s41586-018-0158-3>.
- Kossin, J. P. (2019). Reply to: Moon, I.-J. et al.; Lanzante, J. R. *Nature*, 570(7759), E16–E22. Available from <https://doi.org/10.1038/s41586-019-1224-1>.
- Kossin, J. P., Emanuel, K. A., & Camargo, S. J. (2016). Past and projected changes in Western North Pacific tropical cyclone exposure. *Journal of Climate*, 29(16). Available from <https://doi.org/10.1175/jcli-d-16-0076.1>.
- Kossin, J. P., Emanuel, K. A., & Vecchi, G. A. (2014). The poleward migration of the location of tropical cyclone maximum intensity. *Nature*, 509(7500). Available from <https://doi.org/10.1038/nature13278>.
- Kossin, J. P., Knapp, K. R., Olander, T. L., & Velden, C. S. (2020). Global increase in major tropical cyclone exceedance probability over the past four decades. *Proceedings of the National Academy of Sciences of the United States of America*, 117(22), 11975–11980. Available from <https://doi.org/10.1073/pnas.1920849117>.
- Landsea, C. W., & Franklin, J. L. (2013). Atlantic hurricane database uncertainty and presentation of a new database format. *Monthly Weather Review*, 141(10). Available from <https://doi.org/10.1175/MWR-D-12-00254.1>.
- Landsea, C. W., Vecchi, G. A., Bengtsson, L., & Knutson, T. R. (2010). Impact of duration thresholds on Atlantic tropical cyclone counts. *Journal of Climate*, 23(10). Available from <https://doi.org/10.1175/2009JCLI3034.1>, <http://journals.ametsoc.org/doi/pdf/10.1175/2009JCLI3034.1>, United States.
- Lanzante, J. R. (2019). Uncertainties in tropical-cyclone translation speed. *Nature*, 570(7759), E6. Available from <https://doi.org/10.1038/s41586-019-1223-2>.
- Li, X., Lu, R., Chen, G., & Chen, R. (2023). Tropical cyclones over the South China Sea suppress the monsoonal rainfall in southern China. *npj Climate and Atmospheric Science*, 6(1). Available from <https://doi.org/10.1038/s41612-023-00534-9>.
- Lin, I.-I., Camargo, S. J., Patricola, C. M., Boucharel, J., Chand, S., Klotzbach, P., Chan, J. C. L., Wang, B., Chang, P., Li, T., & Jin, F.-F. (2020). *ENSO and tropical cyclones. El Niño southern oscillation in a changing climate* (pp. 377–408). American Geophysical Union (AGU). Available from <https://doi.org/10.1002/9781119548164.ch17>.
- Lin, N., Kopp, R. E., Horton, B. P., & Donnelly, J. P. (2016). Hurricane Sandy's flood frequency increasing from year 1800 to 2100. *Proceedings of the National Academy of Sciences of the United States of America*, 113(43). Available from <https://doi.org/10.1073/pnas.1604386113>.
- Liu, M., & Smith, J. A. (2016). Extreme rainfall from landfalling tropical cyclones in the eastern United States: Hurricane Irene (2011). *Journal of Hydrometeorology*, 17(11). Available from <https://doi.org/10.1175/JHM-D-16-0072.1>, <http://journals.ametsoc.org/doi/pdf/10.1175/JHM-D-16-0072.1>.
- Liu, M., Vecchi, G. A., Smith, J. A., & Knutson, T. R. (2019). Causes of large projected increases in hurricane precipitation rates with global warming. *npj Climate and Atmospheric Science*, 2(1). Available from <https://doi.org/10.1038/s41612-019-0095-3>, <https://www.nature.com/npjclimatsci/>.

22 Tropical Cyclones and Associated Impacts

- Liu, M., Vecchi, G. A., Smith, J. A., & Murakami, H. (2017). The present-day simulation and twenty-first-century projection of the climatology of extratropical transition in the North Atlantic. *Journal of Climate*, 30(8). Available from <https://doi.org/10.1175/JCLI-D-16-0352.1>, <http://journals.ametsoc.org/doi/pdf/10.1175/JCLI-D-16-0352.1>.
- Liu, M., Vecchi, G. A., Smith, J. A., & Murakami, H. (2018). Projection of landfalling – Tropical cyclone rainfall in the Eastern United States under anthropogenic warming. *Journal of Climate*, 31, 7269–7286. Available from <https://doi.org/10.1175/JCLI-D-17-0747.1>.
- Lonfat, M., Rogers, R., Marchok, T., & Marks, F. D. (2007). A parametric model for predicting hurricane rainfall. *Monthly Weather Review*, 135(9). Available from <https://doi.org/10.1175/mwr3433.1>.
- Lu, K. Y., & Chavas, D. R. (2022). Tropical cyclone size is strongly limited by the Rhines scale: Experiments with a barotropic model. *Journal of the Atmospheric Sciences*, 79(6). Available from <https://doi.org/10.1175/JAS-D-21-0224.1>, <https://journals.ametsoc.org/view/journals/atsc/aop/JAS-D-21-0224.1/JAS-D-21-0224.1.xml>.
- Madden, R. A., & Julian, P. R. (1972). Description of global-scale circulation cells in the tropics with a 40–50 day period. *Journal of the Atmospheric Sciences*, 29(6). Available from [https://doi.org/10.1175/1520-0469\(1972\)029<1109:dogscc>2.0.co;2](https://doi.org/10.1175/1520-0469(1972)029<1109:dogscc>2.0.co;2).
- Mann, M. E., Sabbatelli, T. A., & Neu, U. (2007). Evidence for a modest undercount bias in early historical Atlantic tropical cyclone counts. *Geophysical Research Letters*, 34(22). Available from <https://doi.org/10.1029/2007GL031781>.
- Menemenlis, S., Vecchi, G. A., Gao, K., Smith, J. A., & Cheng, K. (2024). Extreme rainfall risk in Hurricane Ida's extratropical stage: An analysis with convection-permitting ensemble hindcasts. *Journal of the Atmospheric Sciences*. Available from <https://doi.org/10.1175/JAS-D-23-0160.1>.
- Moon, I.-J., Sung-Hun Kim., & Chan, J. C. L. (2019). Climate change and tropical cyclone trend. *Nature*, 570(7759), E3–E5. Available from <https://doi.org/10.1038/s41586-019-1222-3>.
- Mostert, W., Popinet, S., & Deike, L. (2022). High-resolution direct simulation of deep water breaking waves: Transition to turbulence, bubbles and droplets production. *Journal of Fluid Mechanics*, 942, A27. Available from <https://doi.org/10.1017/jfm.2022.330>.
- Murakami, H., Vecchi, G. A., Delworth, T. L., Paffendorf, K., Gudgel, R., Jia, L., & Zeng, F. (2015). Investigating the influence of anthropogenic forcing and natural variability on the 2014 Hawaiian hurricane season. *Bulletin of the American Meteorological Society*, 96(12), S115. Available from <https://doi.org/10.1175/BAMS-D-15-00119.1>, http://journals.ametsoc.org/doi/pdf/10.1175/BAMS-EEE_2014_ch23.1.
- Murakami, H., Vecchi, G. A., Delworth, T. L., Wittenberg, A. T., Underwood, S., Gudgel, R., Yang, X., Jia, L., Zeng, F., Paffendorf, K., & Zhang, W. (2017). Dominant role of subtropical pacific warming in extreme Eastern Pacific hurricane seasons: 2015 and the future. *Journal of Climate*, 30(1). Available from <https://doi.org/10.1175/JCLI-D-16-0424.1>, <http://journals.ametsoc.org/doi/pdf/10.1175/JCLI-D-16-0424.1>.
- Murakami, H., Villarini, G., Vecchi, G. A., Zhang, W., & Gudgel, R. (2016). Statistical-dynamical seasonal forecast of North Atlantic and U.S. land-falling tropical cyclones using the high-resolution GFDL FLOR coupled model. *Monthly Weather Review*, 144(6). Available from <https://doi.org/10.1175/MWR-D-15-0308.1>, <http://journals.ametsoc.org/doi/pdf/10.1175/MWR-D-15-0308.1>.
- Murakami, H., & Wang, B. (2022). Patterns and frequency of projected future tropical cyclone genesis are governed by dynamic effects. *Communications Earth & Environment*, 3(1). Available from <https://doi.org/10.1038/s43247-022-00410-z>.
- Murakami, M. (1976). Analysis of summer monsoon fluctuations over India. *Journal of the Meteorological Society of Japan. Ser. II*, 54(1). Available from https://doi.org/10.2151/jmsj1965.54.1_15.
- National Hurricane Center. (Updated May 2021). *The Saffir–Simpson Hurricane Wind Scale*.
- Nederhoff, K., Leijnse, T. W. B., Parker, K., Thomas, J., O'Neill, A., van Ormondt, M., McCall, R., Erikson, L., Barnard, P. L., Foxgrover, A., Klessens, W., Nadal-Caraballo, N. C., & Massey, T. C. (2024). Tropical or extratropical cyclones: What drives the compound flood hazard, impact, and risk for the United States Southeast Atlantic coast? *Natural Hazards*. Available from <https://doi.org/10.1007/s11069-024-06552-x>, <https://www.springer.com/journal/11069>.
- Orton, P. M., Hall, T. M., Talke, S. A., Blumberg, A. F., Georgas, N., & Vinogradov, S. (2016). A validated tropical-extratropical flood hazard assessment for New York Harbor. *Journal of Geophysical Research: Oceans*, 121(12). Available from <https://doi.org/10.1002/2016JC011679>, [http://onlinelibrary.wiley.com/journal/10.1002/\(ISSN\)2169-9291](http://onlinelibrary.wiley.com/journal/10.1002/(ISSN)2169-9291).
- Pegion, K., Kirtman, B. P., Becker, E., Collins, D. C., LaJoie, E., Burgman, R., Bell, R., DelSole, T., Min, D., Zhu, Y., Li, W., Sinsky, E., Guan, H., Gottschalck, J., Metzger, E. J., Barton, N. P., Achuthavarier, D., Marshak, J., Koster, R. D., ... Kim, H. (2019). The Subseasonal Experiment (SubX): A multimodel subseasonal prediction experiment. *Bulletin of the American Meteorological Society*, 100(10). Available from <https://doi.org/10.1175/bams-d-18-0270.1>.
- Peng, T., & Richter, D. (2019). Sea spray and its feedback effects: Assessing bulk algorithms of air–sea heat fluxes via direct numerical simulations. *Journal of Physical Oceanography*, 49(6). Available from <https://doi.org/10.1175/JPO-D-18-0193.1>, <https://journals.ametsoc.org/doi/pdf/10.1175/JPO-D-18-0193.1>.
- Popinet, S. (2009). An accurate adaptive solver for surface-tension-driven interfacial flows. *Journal of Computational Physics*, 228(16). Available from <https://doi.org/10.1016/j.jcp.2009.04.042>.
- Popol Vuh: The sacred book of the Maya (A. J. Christenson, Trans.). (2007). University of Oklahoma Press.
- Popinet, S. (2020). A vertically-Lagrangian, non-hydrostatic, multilayer model for multiscale free-surface flows. *Journal of Computational Physics*, 418. Available from <https://doi.org/10.1016/j.jcp.2020.109609>.
- Price, J. F. (1981). Upper ocean response to a hurricane. *Journal of Physical Oceanography*, 11(2). Available from [https://doi.org/10.1175/1520-0485\(1981\)011<0153:uoratah>2.0.co;2](https://doi.org/10.1175/1520-0485(1981)011<0153:uoratah>2.0.co;2).
- Pérez-Alarcón, A., Coll-Hidalgo, P., Fernández-Alvarez, J. C., Trigo, R. M., Nieto, R., & Gimeno, L. (2023). Impacts of tropical cyclones on the global water budget. *npj Climate and Atmospheric Science*, 6(1). Available from <https://doi.org/10.1038/s41612-023-00546-5>.
- Ramsay, H. (2017). *The global climatology of tropical cyclones*. Oxford research encyclopedia of natural hazard science. Oxford University Press. Available from <http://doi.org/10.1093/acrefore/9780199389407.013.79>.

- Rappin, E. D., Nolan, D. S., & Emanuel, K. A. (2010). Thermodynamic control of tropical cyclogenesis in environments of radiative-convective equilibrium with shear. *Quarterly Journal of the Royal Meteorological Society*, 136, 1954–1971. Available from <https://doi.org/10.1002/qj.706>.
- Richter, D. H., & Wainwright, C. E. (2023). Large-Eddy simulation of sea spray impacts on fluxes in the high-wind boundary layer. *Geophysical Research Letters*, 50(3). Available from <https://doi.org/10.1029/2022GL101862>, [http://agupubs.onlinelibrary.wiley.com/hub/journal/10.1002/\(ISSN\)1944-8007](http://agupubs.onlinelibrary.wiley.com/hub/journal/10.1002/(ISSN)1944-8007).
- Rivièvre, A., Mostert, W., Perrard, S., & Deike, L. (2021). Sub-Hinze scale bubble production in turbulent bubble break-up. *Journal of Fluid Mechanics*, 917, A40. Available from <https://doi.org/10.1017/jfm.2021.243>.
- Rivièvre, A., Ruth, D. J., Mostert, W., Deike, L., & Perrard, S. (2022). Capillary driven fragmentation of large gas bubbles in turbulence. *Physical Review Fluids*, 7(8). Available from <https://doi.org/10.1103/PhysRevFluids.7.083602>, <https://journals.aps.org/prfluids/abstract/10.1103/PhysRevFluids.7.083602>.
- Rotunno, R., & Emanuel, K. A. (1987). An air-sea interaction theory for tropical cyclones. Part II: Evolutionary study using a nonhydrostatic axisymmetric numerical model. *Journal of the Atmospheric Sciences*, 44(3). Available from [https://doi.org/10.1175/1520-0469\(1987\)044<0542:AAITFT>2.0.CO;2](https://doi.org/10.1175/1520-0469(1987)044<0542:AAITFT>2.0.CO;2).
- Scapin, N. (2022). *Phase-changing flows: Numerical methods and fully resolved simulations* [Dissertation, KTH Royal Institute of Technology].
- Scapin, N., Costa, P., & Brandt, L. (2020). A volume-of-fluid method for interface-resolved simulations of phase-changing two fluid flows. *Journal of Computational Physics*, 407, 109251. Available from <https://doi.org/10.1016/j.jcp.2020.109251>.
- Scapin, N., Demou, A., & Brandt, L. (2023). *Journal of Fluid Mechanics*, 957, A12. Available from <https://doi.org/10.1017/jfm.2023.57>.
- Schreck, C. J., Vitart, F., Camargo, S. J., Camp, J., Darlow, J., Elsberry, R., Gottschalck, J., Gregory, P., Hansen, K., Jackson, J., Janiga, M. A., Klotzbach, P. J., Lee, C.-Y., Long, L., Nakano, M., Takemura, K., Takaya, Y., Ventrice, M. J., & Wang, Z. (2023). Advances in tropical cyclone prediction on subseasonal time scales during 2019–2022. *Tropical Cyclone Research and Review*, 12(2). Available from <https://doi.org/10.1016/j.tcr.2023.06.004>.
- Schwartz, S. B. (2015). *Sea of storms: A history of hurricanes in the Greater Caribbean from Columbus to Katrina*. Princeton University Press. Available from <http://press.princeton.edu/titles/10324.html>.
- Schwerdt, R. W., Ho, F. P., Watkins, R. R. (1979). *Meteorological criteria for standard project hurricane and probable maximum hurricane wind fields, gulf and east coasts of the United States*. NOAA technical report, NWS 23. U.S. Department of Commerce, National Oceanic and Atmospheric Administration, National Weather Service, Washington, D.C.
- Scoccimarro, E., Gualdi, S., Bellucci, A., Peano, D., Cherchi, A., Vecchi, G. A., & Navarra, A. (2020). The typhoon-induced drying of the Maritime Continent. *Proceedings of the National Academy of Sciences of the United States of America*, 117(8). Available from <https://doi.org/10.1073/pnas.1915364117>, <https://www.pnas.org/content/pnas/117/8/3983.full.pdf>.
- Scoccimarro, E., Gualdi, S., Bellucci, A., Sanna, A., Fogli, P. G., Manzini, E., Vichi, M., Oddo, P., & Navarra, A. (2011). Effects of tropical cyclones on ocean heat transport in a high-resolution coupled general circulation model. *Journal of Climate*, 24(16). Available from <https://doi.org/10.1175/2011JCLI4104.1Italy>, <http://journals.ametsoc.org/doi/pdf/10.1175/2011JCLI4104.1>.
- Sriver, R. L., & Huber, M. (2010). Modeled sensitivity of upper thermocline properties to tropical cyclone winds and possible feedbacks on the Hadley circulation. *Geophysical Research Letters*, 37(8). Available from <https://doi.org/10.1029/2010GL042836>.
- Sroka, S., & Emanuel, K. (2021). A review of parameterizations for enthalpy and momentum fluxes from sea spray in tropical cyclones. *Journal of Physical Oceanography*, 51(10), 3053–3069. Available from <https://doi.org/10.1175/JPO-D-21-0023.1>.
- Staten, P. W., Grise, K. M., Davis, S. M., Karnauskas, K. B., Waugh, D. W., Maycock, A. C., Fu, Q., Cook, K., Adam, O., Simpson, I. R., Allen, R. J., Rosenlof, K., Chen, G., Ummenhofer, C. C., Quan, X.-W., Kossin, J. P., Davis, N. A., & Son, S.-W. (2020). Tropical widening: From global variations to regional impacts. *Bulletin of the American Meteorological Society*, 101(6), E897. Available from <https://doi.org/10.1175/bams-d-19-0047.1>.
- Stramma, L., Cornillon, P., & Price, J. F. (1986). Satellite observations of sea surface cooling by hurricanes. *Journal of Geophysical Research*, 91 (C4), 5031–5035. Available from <https://doi.org/10.1029/JC091iC04p05031>.
- Sullivan, P. P., Edson, J. B., Hristov, T., & McWilliams, J. C. (2008). Large-eddy simulations and observations of atmospheric marine boundary layers above nonequilibrium surface waves. *Journal of the Atmospheric Sciences*, 65(4). Available from <https://doi.org/10.1175/2007JAS2427.1>, <http://ams.allenpress.com/archive/1520-0469/65/4/pdf/i1520-0469-65-4-1225.pdf>, United States.
- Sun, Y., Zhong, Z., Li, T., Yi, L., Hu, Y., Wan, H., Chen, H., Liao, Q., Ma, C., & Li, Q. (2017). Impact of ocean warming on tropical cyclone size and its destructiveness. *Scientific Reports*, 7(1). Available from <https://doi.org/10.1038/s41598-017-08533-6>.
- Tang, B., & Emanuel, K. (2010). Midlevel ventilation's constraint on tropical cyclone intensity. *Journal of the Atmospheric Sciences*, 67(6). Available from <https://doi.org/10.1175/2010JAS3318.1>, <http://journals.ametsoc.org/doi/pdf/10.1175/2010JAS3318.1>, United States.
- Tang, B. H., & Neelin, J. D. (2004). ENSO influence on Atlantic hurricanes via tropospheric warming. *Geophysical Research Letters*, 31(24). Available from <https://doi.org/10.1029/2004gl021072>.
- Tippett, M. K., Camargo, S. J., & Sobel, A. H. (2011). A Poisson regression index for tropical cyclone genesis and the role of large-scale vorticity in genesis. *Journal of Climate*, 24(9). Available from <https://doi.org/10.1175/2010jcli3811.1>.
- Vecchi, G. A., Delworth, T., Gudgel, R., Kapnick, S., Rosati, A., Wittenberg, A. T., Zeng, F., Anderson, W., Balaji, V., Dixon, K., Jia, L., Kim, H.-S., Krishnamurthy, L., Msadek, R., Stern, W. F., Underwood, S. D., Villarini, G., Yang, X., & Zhang, S. (2014). On the seasonal forecasting of regional tropical cyclone activity. *Journal of Climate*, 27(21). Available from <https://doi.org/10.1175/jcli-d-14-00158.1>.
- Vecchi, G. A., & Knutson, T. R. (2008). On estimates of historical North Atlantic tropical cyclone activity. *Journal of Climate*, 21(14). Available from <https://doi.org/10.1175/2008JCLI2178.1>, <http://ams.allenpress.com/perlserv/?request=res-loc&uri=urn%3Aap%3Apdf%3Adoi%3A10.1175%2F2008JCLI2178.1>, United States.

24 Tropical Cyclones and Associated Impacts

- Vecchi, G. A., & Knutson, T. R. (2011). Estimating annual numbers of Atlantic hurricanes missing from the HURDAT database (1878–1965) using ship track density. *Journal of Climate*, 24(6). Available from <https://doi.org/10.1175/2010JCLI3810.1>, <http://journals.ametsoc.org/doi/pdf/10.1175/2010JCLI3810.1>, United States.
- Vecchi, G. A., Landsea, C., Zhang, W., Villarini, G., & Knutson, T. (2021). Changes in Atlantic major hurricane frequency since the late-19th century. *Nature Communications*, 12(1). Available from <https://doi.org/10.1038/s41467-021-24268-5>, <http://www.nature.com/ncomms/index.html>.
- Vecchi, G. A., & Villarini, G. (2014). Next season's hurricanes. *Science (New York, N.Y.)*, 343(6171). Available from <https://doi.org/10.1126/science.1247759>, <http://www.sciencemag.org/content/343/6171/618.full.pdf>.
- Vecchi, G. A., Zhao, M., Wang, H., Villarini, G., Rosati, A., Kumar, A., Held, I. M., & Budde, R. (2011). Statistical-dynamical predictions of seasonal North Atlantic hurricane activity. *Monthly Weather Review*, 139(4). Available from <https://doi.org/10.1175/2010MWR3499.1>, <http://journals.ametsoc.org/doi/pdf/10.1175/2010MWR3499.1>, United States.
- Veron, F. (2015). Ocean spray. *Annual Review of Fluid Mechanics*, 47, 507–538. Available from <https://doi.org/10.1146/annurev-fluid-010814-014651>.
- Villarini, G., Luitel, B., Vecchi, G. A., & Ghosh, J. (2019). Multi-model ensemble forecasting of North Atlantic tropical cyclone activity. *Climate Dynamics*, 53(12). Available from <https://doi.org/10.1007/s00382-016-3369-z>, <http://link.springer.de/link/service/journals/00382/index.htm>.
- Villarini, G., Vecchi, G. A., Knutson, T. R., & Smith, J. A. (2011). Is the recorded increase in short-duration North Atlantic tropical storms spurious? *Journal of Geophysical Research Atmospheres*, 116(10). Available from <https://doi.org/10.1029/2010JD015493>, [http://onlinelibrary.wiley.com/journal/10.1002/\(ISSN\)2169-8996](http://onlinelibrary.wiley.com/journal/10.1002/(ISSN)2169-8996).
- Vimont, D. J., & Kossin, J. P. (2007). The Atlantic Meridional Mode and hurricane activity. *Geophysical Research Letters*, 34(7). Available from <https://doi.org/10.1029/2007GL029683>.
- Vitart, F., & Robertson, A. W. (2018). The sub-seasonal to seasonal prediction project (S2S) and the prediction of extreme events. *npj Climate and Atmospheric Science*, 1(1). Available from <https://doi.org/10.1038/s41612-018-0013-0>, <http://www.nature.com/npjclimatesci/>.
- Walsh, K. J. E., Camargo, S. J., Knutson, T. R., Kossin, J., Lee, T.-C., Murakami, H., & Patricola, C. (2019). Tropical cyclones and climate change. *Tropical Cyclone Research and Review*, 8(4). Available from <https://doi.org/10.1016/j.tcr.2020.01.004>.
- Wang, B., Li, X., & Wu, L. (1997). Direction of hurricane beta drift in horizontally sheared flows. *Journal of the Atmospheric Sciences*, 54, 1462–1471. Available from <http://journals.ametsoc.org/loi/atsc>, [https://doi.org/10.1175/1520-0469\(1997\)054<1462:DOHBDI>2.0.CO;2](https://doi.org/10.1175/1520-0469(1997)054<1462:DOHBDI>2.0.CO;2).
- Wang, B., & Murakami, H. (2020). Dynamic genesis potential index for diagnosing present-day and future global tropical cyclone genesis. *Environmental Research Letters*, 15(11), 114008. Available from <https://doi.org/10.1088/1748-9326/abbb01>.
- Wang, G., Wu, L., Mei, W., & Xie, S.-P. (2022). Ocean currents show global intensification of weak tropical cyclones. *Nature*, 611(7936). Available from <https://doi.org/10.1038/s41586-022-05326-4>.
- Wehner, M. F., & Kossin, J. P. (2024). The growing inadequacy of an open-ended Saffir–Simpson hurricane wind scale in a warming world. *Proceedings of the National Academy of Sciences of the United States of America*, 121(7). Available from <https://doi.org/10.1073/pnas.2308901121>.
- Wing, A. A., Camargo, S. J., & Sobel, A. H. (2016). Role of radiative–convective feedbacks in spontaneous tropical cyclogenesis in idealized numerical simulations. *Journal of the Atmospheric Sciences*, 73(7), 2633–2642. Available from <https://doi.org/10.1175/JAS-D-15-0380.1>.
- Wing, A. A., Camargo, S. J., Sobel, A. H., Kim, D., Moon, Y., Murakami, H., Reed, K. A., Vecchi, G. A., Wehner, M. F., Zarzycki, C., & Zhao, M. (2019). Moist static energy budget analysis of tropical cyclone intensification in high-resolution climate models. *Journal of Climate*, 32(18). Available from <https://doi.org/10.1175/JCLI-D-18-0599.1>, <http://journals.ametsoc.org/loi/clim>.
- Wright, D. B., Knutson, T. R., & Smith, J. A. (2015). Regional climate model projections of rainfall from U.S. landfalling tropical cyclones. *Climate Dynamics*, 45(11), 3365–3379. Available from <https://doi.org/10.1007/s00382-015-2544-y>.
- Wu, J., & Deike, L. (2021). Wind wave growth in the viscous regime. *Physical Review Fluids*, 6(9). Available from <https://doi.org/10.1103/physrevfluids.6.094801>.
- Wu, J., Popinet, S., & Deike, L. (2022). Revisiting wind wave growth with fully coupled direct numerical simulations. *Journal of Fluid Mechanics*, 951, A18. Available from <https://doi.org/10.1017/jfm.2022.822>.
- Wu, J., Popinet, S., & Deike, L. (2023). Breaking wave field statistics with a multi-layer model. *Journal of Fluid Mechanics*, 968, A12. Available from <https://doi.org/10.1017/jfm.2023.522>.
- Xie, Y.-B., Chen, S.-J., Zhang, I.-L., & Hung, Y.-L. (1963). A preliminary statistic and synoptic study about the basic currents over southeastern Asia and the initiation of typhoon. *Acta Meteorologica Sinica*, 33. Available from <https://doi.org/10.11676/qxxb1963.020>.
- Yang, W., Hsieh, T.-L., & Vecchi, G. A. (2021). Hurricane annual cycle controlled by both seeds and genesis probability. *Proceedings of the National Academy of Sciences of the United States of America*, 118(41), e2108397118. Available from <https://doi.org/10.1073/pnas.2108397118>.
- Yang, W., Vecchi, G. A., Fueglistaler, S., Horowitz, L. W., Luet, D. J., Muñoz, Á. G., Paynter, D., & Underwood, S. (2019). Climate impacts from large volcanic eruptions in a high-resolution climate model: The importance of forcing structure. *Geophysical Research Letters*, 46(13). Available from <https://doi.org/10.1029/2019GL082367>.
- Yang, W., Wallace, E., Vecchi, G. A., Donnelly, J. P., Emile-Geay, J., Hakim, G. J., Horowitz, L. W., Sullivan, R. M., Tardif, R., van Hengstum, P. J., & Winkler, T. S. (2024). Last millennium hurricane activity linked to endogenous climate variability. *Nature Communications*, 15(1). Available from <https://doi.org/10.1038/s41467-024-45112-6>, <http://www.nature.com/ncomms/>.
- You, L., Gao, J., Lin, H., & Chen, S. (2019). Impact of the intra-seasonal oscillation on tropical cyclone genesis over the western North Pacific. *International Journal of Climatology*, 39(4). Available from <https://doi.org/10.1002/joc.5927>.
- Zhang, B., Soden, B. J., Vecchi, G. A., & Yang, W. (2021). The role of radiative interactions in tropical cyclone development under realistic boundary conditions. *Journal of Climate*, 34(6). Available from <https://doi.org/10.1175/JCLI-D-20-0574.1>, <https://journals.ametsoc.org/view/journals/clim/34/6/JCLI-D-20-0574.1.xml>.

- Zhang, D., Zhang, H., Zheng, J., Cheng, X., Tian, D., & Chen, D. (2020). Changes in tropical-cyclone translation speed over the Western North Pacific. *Atmosphere*, 11(1), 93. Available from <https://doi.org/10.3390/atmos11010093>.
- Zhang, W., Vecchi, G. A., Villarini, G., Murakami, H., Rosati, A., Yang, X., Jia, L., & Zeng, F. (2017). Modulation of western North Pacific tropical cyclone activity by the Atlantic Meridional Mode. *Climate Dynamics*, 48(1), 631–647. Available from <https://doi.org/10.1007/s00382-016-3099-2>.
- Zhang, G., Wang, Z., Peng, M. S., & Magnusdottir, G. (2017). Characteristics and impacts of extratropical Rossby wave breaking during the Atlantic hurricane season. *Journal of Climate*, 30(7). Available from <https://doi.org/10.1175/JCLI-D-16-0425.1>, <http://journals.ametsoc.org/doi/pdf/10.1175/JCLI-D-16-0425.1>.
- Zhou, L., Lin, S. J., Chen, J. H., Harris, L. M., Chen, X., & Rees, S. L. (2019). Toward convective-scale prediction within the next generation global prediction system. *Bulletin of the American Meteorological Society*, 100(7). Available from <https://doi.org/10.1175/BAMS-D-17-0246.1>, <https://journals.ametsoc.org/doi/pdf/10.1175/BAMS-D-17-0246.1>.